

Interactive comment on “On constraining the strength of the terrestrial CO₂ fertilization effect in an Earth system model” by V. K. Arora and J. F. Scinocca

V. K. Arora and J. F. Scinocca

vivek.arora@ec.gc.ca

Received and published: 9 May 2016

We thank our reviewers for their constructive and detailed comments. Our responses to reviewers' comments are indicated in **bold font** and indented, while reviewers' comments are shown in a regular font.

Reviewer # 1

In this manuscript, the authors attempted to constrain a parameter of the Canadian Earth System Model version 4.2 in terms of atmospheric CO₂ fertilization effect, which is one of the most uncertain process in the future climate–carbon cycle feedback. By conducting a series of simulations using different parameter values ($\gamma_d = 0.25, 0.4, 0.55$), they chose the most plausible parameter value that allows most

C1

realistic simulations of atmospheric CO₂ growth and its seasonal amplitude. Apparently, this is an up-to-date and meaningful work to improve the reliability of Earth System Models. The new experiment, “relaxed-CO₂”, is especially interesting for me. The manuscript was clearly written and I found no logical fault. Nevertheless, I have a few moderate caveats on this study.

First, the CO₂ fertilization parameter (γ_d) represents photosynthetic down-regulation (not the fertilization effect itself) in an empirical manner. So, the selected parameter value (i.e., 0.4) seems to be specific to the CanESM4.2.

Thank you pointing this. Yes, indeed the γ_d parameter is related to down-regulation. A smaller value of γ_d indicates more down-regulation, and a higher value of γ_d indicates higher strength of the CO₂ fertilization effect. We now make this clear in the revised manuscript. Also, as we mention later in response to reviewer # 3, while the parameter γ_d is specific to our model, it is the rate of increase of NPP that is relevant to other modellers and the community at large.

Second, this study compared only three parameter values, and so the selected one (0.4) may not be exactly the best one.

It wasn't our objective to run the model for tens of possible values of the γ_d parameter. Rather, the objective of the manuscript is to illustrate how this parameter can be adjusted in the framework of our model to best reproduce aspects of the global carbon cycle and the historical carbon budget.

Third, recently, Schimel et al. (2015) published a very relevant paper on constraining the CO₂ fertilization effect, but this was not referred in the manuscript.

The Schimel et al. (2015) paper focusses on the relative roles of tropical and extra-tropical terrestrial carbon sinks but does not explicitly attempts to constrain the strength of the CO₂ fertilization effect. Yet, it's a relevant paper and we now mention this in the introductory section.

In conclusion, the manuscript is well prepared and may be accepted for publication after moderate revision.

Thank you.

Specific comments are given below.

Page 4 Line 21–26: Several studies used FACE data for benchmarking of terrestrial vegetation models (Piao et al., 2013; Zaehle et al., 2014).

C2

Reviewer # 3 mentions that the traditional and more widely followed approach of model evaluation and parameter calibration is where process level understanding can be gained. This is in contrast to our top-down kind of approach where we evaluate an emergent property at the global scale. The Zaehle et al. (2014) reference is now mentioned in the discussions and the conclusions section, in the context of evaluating models for gaining understanding at the process level.

Page 12 Line 24: How the default parameter of CanESM2 ($\gamma_d = 0.25$) was determined?

For CanESM2 we used only two determinants to determine the value of γ_d parameter – globally averaged surface CO₂ and cumulative atmosphere-land CO₂ flux. CanESM2 wasn't as rigorously evaluated. This is now clarified in the revised manuscript.

Page 19 Line 25: Remove the space between “under” and “predict”.

Thank you for noting this. This has been corrected.

Reviewer # 2

Authors present in this paper the structure of the new Earth system model developed in CCCma, and then they attempt to evaluate the model's performance to reproduce the global carbon budget and atmospheric CO₂ concentration during 1850-2005 periods, with simulation ensembles and different parameters/configurations. In their evaluation, they focus on particularly the land ecosystem process so called “CO₂ fertilization effect”, which is strongly associated with the most uncertain feedback process within the global carbon cycle. It is noteworthy that the authors consider four types of observation constraints in their model evaluation, which makes their conclusions more robust. Overall, this paper is clearly written and well structured, and will contribute to the journal. Detailed comments are listed below, and I believe most of them will not require much effort to improve.

p4, L7- “the uncertainty in the carbon-concentration feedback over land had somewhat reduced since the first coupled carbon cycle climate model intercomparison project (C4MIP)” I'm afraid this sentence might mislead readers. Since the 1st and 2nd MIP used different scenarios (SRES-A2 / 1pctCO₂) and configurations (emission/concentration-driven) to evaluate carbon cycle feedbacks, we cannot directly compare the feedback strength between the two MIPs.

Yes, it is true that the first C4MIP study was performed for the SRES A2 scenario while Arora et al. (2013) used results from the 1% per year increasing CO₂ simulation. This means that the average strengths of feedbacks cannot be compared across the two studies. However,

C3

our sentence attempts to compares the uncertainty in calculated values of the feedback parameters as indicated by their standard deviation. This is now clarified in the revised manuscript.

P10, L23- It will be helpful for readers to briefly mention the decay-timescale of the pools for “short” and “long” (: from Arora and Boer 2011, it seems the two product pools are equivalent to litter/soil). This information will be helpful to understand the reduction of soil carbon mass in LUC simulation and the delayed response of soil carbon pools (Fig. 5c).

Yes, the short and long time scales for the land use change (LUC) products correspond to time scales of the litter and soil carbon pools. This is now mentioned in the revised manuscript.

P23 L19; p24 L10; p27 L5 Should these “CanESM2” be replaced by “CanESM4.2” ?

Thank you for noting these typos.

P24 L28- p25 L2 In my understanding, your choice of “emission-driven” configuration might be one of the reasons to underestimate the LUC emission (EL): since LUC emission is omitted in the “without LUC experiments”, the CO₂ concentration stays lower level and the CO₂ fertilization effect becomes weaker. As a result, the cumulative land carbon uptake in the “without LUC” experiment (FL) is more or less underestimated, which yields lower EL (=FL' - FL). I recommend the authors to mention this.

When LUC emissions are determined by differencing atmosphere-land CO₂ flux from simulations with and without LUC, then the diagnosed LUC emissions depend on how simulations are performed. It is correct, that if concentration-driven simulations were to be used the diagnosed LUC emissions would have been higher and closer to Houghton (2008) estimates. We have now added additional text in the manuscript to clarify this.

Discussion section

As commented above, simulations without LUC inevitably lead to lower CO₂ concentration and weaker CO₂ fertilization effect. I think this can be a “noise” when evaluating LUC emission/impacts. Specifically, in Fig.4(b), NPP in “without LUC” simulation are generally lower than “with LUC”, but it is difficult to identify the reason of the difference, because the NPP difference can be affected by CO₂ fertilization, increased GPP by crops, and vegetation regrowth. I hope the authors to make a few discussions about the configuration settings for evaluating LUC impacts. I believe such information will be helpful when making simulation designs in the coming CMIP.

We do not think that, when evaluating LUC emissions as the difference between

C4

atmosphere-land CO₂ flux in emissions-driven simulations with and without LUC, the lower CO₂ concentration in simulations without LUC can be considered as noise. In fact, lower CO₂ concentration in simulations without LUC, is expected and it is systematic. As reviewer # 3 suggested, our simulations could have been performed for the concentration-driven case. In that case, the diagnosed LUC emissions would have been higher and closer to Houghton (2008) estimates (as we mentioned above) and the difference in the rate of increase of NPP in simulations with and without LUC would have been solely due to differences in land cover. However, we would not have been able to use the fourth criterion, i.e. the amplitude of the annual CO₂ cycle and its rate of increase, to assess our simulations.

As mentioned above, we now mention in the revised manuscript what the LUC emissions would have been had we use concentration-driven simulations. However, we feel that while concentration-driven simulations make interpretation of results easier, emissions-driven simulations are more appropriate for our context. The real-world system is, of course, emissions-driven.

In Fig.2, $\gamma_d = 0.25$ simulations display moderate land carbon sink among CMIP5-ESMs. I think this result is reasonable because most CMIP5-ESMs may not consider down-regulation mechanism; Fig.9 also supports the choice of the parameter value. However, the historical simulations with $\gamma_d = 0.25$ did not do a good job for reproducing land carbon uptake (Fig. 4). Although you discussed on this in the text, I suppose we have two more things to discuss. The first is the additional carbon uptake by vegetation regrowth. Although the regrowth mechanisms in the model are presented on p10-11, I'm not sure if the modeling was appropriate or not. If we can expect more carbon gain by vegetation regrowth, simulations with $\gamma_d = 0.25$ may work better. The second is the parameter value of humification factor. If you choose more moderate value for the humification factor (or modify the fractions of deforested/removed biomass that goes into fast/slow pools), soil carbon mass displayed in Fig. 5c will push up toward positive, and this treatment will also make the simulation with $\gamma_d = 0.25$ more realistic. I hope to see some discussions on these two points.

This comment is somewhat unclear. The terrestrial ecosystem model used in our Earth system model grows vegetation in response to environmental conditions including atmospheric CO₂ concentration. Once the model reaches equilibrium, e.g. for environmental conditions corresponding to 1850, then a change in climate and/or atmospheric CO₂ concentration will make the model lose or gain carbon. Since CO₂ increases over the historical period then in a globally-averaged sense the model gains carbon creating the land carbon sink. We are unsure what "other" mechanisms can be used to grow vegetation.

As mentioned earlier, even if other models do not incorporate down-regulation it's the rate

C5

of increase of NPP over the historical period that is relevant here.

The second part of this comment raises the dilemma our study illustrates. Yes, we can use a moderate value of the humification factor between 0.1 and 0.45 and use a lower value of γ_d but that would yield lower soil carbon loss due to anthropogenic LUC and the carbon uptake for decades of 1960s through 2000s will likely not compare well with observation-based estimates from Le Quere et al. (2015), as was the case for CanESM2.

The other dilemma we faced is that while $\gamma_d = 0.4$ yields the best possible comparison with observation-based determinants of the global carbon cycle and historical carbon budget the model now yields carbon uptake that is highest amongst all CMIP5 models. This does not indicate that CanESM4.2 simulation of the historical carbon budget is grossly incorrect, but does make us an outlier amongst CMIP5 models.

About Title:

I'm thinking the key feature of this paper is constraining the historical carbon budget of the model from different angles. Of course, it is necessary for your model to choose an appropriate value for the down-regulation, but its parameterization looks somewhat specific to your model. My suggestion is to change the title to reflect "CO₂ fertilization", "LUC", and "historical carbon budget": I believe these are the main issues in the background and will have more meaningful messages for readers.

While a valid suggestion, we feel the current title of the manuscript conveys the primary intent of the manuscript.

Reviewer # 3

Overall comment: This is an interesting study and asks an important question: how can we constrain an emergent property such as the global responsiveness to elevated CO₂ based on global transient observational records? The authors are careful to emphasize the contingent nature of their answers, and emphasize that such answers cannot be unambiguously identified by this approach due to the presence of large amounts of model and forcing uncertainty that determine the response. I would personally go further and ask whether it makes sense at all to try to "tune" emergent model properties to match transient data in such an explicit manner. The more widely-followed approach is to test model components at scales where process-level understanding can be gained, in hopes of removing some of the dependence on overall model behavior that may influence results, for example by comparing at FACE sites (e.g. the various FACE-MIP papers), or by systematically benchmarking multiple aspects of the model in order to better understand the structural control on emergent behaviors. So while I do see this paper as a valuable

C6

contribution, I also feel that, in the end, the answer to the problem posed in the title is that it very much depends on what is in the ESM itself, and so without understanding how accurate the model is across a wide range of predictions, it is impossible to know whether the specific answer inferred by the comparison is informative of the real world or not.

Thank you for your interesting view point. Yes, it is true that traditionally models are evaluated using the bottom-up approach where aspects of the model are compared with observations to assess its various process-based parameterizations. The Canadian terrestrial ecosystem model (CTEM), which is the terrestrial carbon cycle component of CanESM4.2, has indeed been evaluated at point (e.g. Arora and Boer, 2005; Melton et al., 2015), regional (e.g. Peng et al., 2014; Garnaud et al., 2014) and global (e.g. Arora and Boer, 2010; Melton and Arora, 2014) scales in a number of studies. In regards to the CO₂ fertilization effect, based on results from FACE and other studies that grew plants at ambient and elevated CO₂, Arora et al. (2009) obtained a value of γ_d equivalent to about 0.46 for use in CTEM.

Just like top-down inversion-based studies are complementary to bottom-up studies (e.g. those which measure forest stem growth rates) in determining spatial distribution of carbon sinks and sources, we believe that there is value in evaluating and “tuning” CTEM using a top-down approach, as in our study, against an emergent model property. Amongst model simulations performed for our study for $\gamma_d = 0.25, 0.4$ and 0.55 , the simulation with $\gamma_d = 0.4$ yields the best comparison with observation-based estimates. Indeed our “best” γ_d of 0.4 is broadly consistent with Arora et al. (2009) derived γ_d of 0.46 based on FACE studies.

The tuned value of γ_d is indeed model-dependent and we do mention this on top of page 26 of the discussion paper. To place confidence in the model, however, we attempt to compare different aspects of the model with observation-based estimates. These include loss in the global soil carbon amount due to anthropogenic LUC and the amplitude of annual CO₂ cycle and its rate of increase over the historical period.

Finally, while the γ_d parameter is specific to our model what’s more useful for other modellers and the community at large is the simulated rate of increase of NPP over the historical period (which we explicitly mention in our abstract). The rate of increase of NPP can be directly compared across different models.

These points have now been clarified in the revised manuscript.

page 5, lines 7-14: I don’t see how, from the perspective of the terrestrial biosphere, the information content of the first three of these tests are different. So if the focus is just on the land, why include the total CO₂ growth rate at all since the answer is affected by the uncertainty in ocean and fossil fuel

C7

emissions?

Ignoring, the CO₂ growth rate over the historical period, against which model simulations are assessed, is certainly possible but that will make the simulations concentration-driven instead of being emissions-driven (which is what we have used in our study). The caveat with concentration-driven simulations is that it wouldn’t be possible to analyze and use the amplitude of the annual CO₂ cycle and its rate of increase over the historical period to evaluate the model. Concentration-driven simulations either ignore the annual cycle of CO₂ (our specified-CO₂ case) or use a specified amplitude of the CO₂ annual cycle (our relaxed-CO₂ case). We do see value in comparing simulated and observed amplitude of the annual CO₂ cycle and its rate of increase over the historical period.

The information in cumulative atmosphere-land CO₂ flux for the period 1850-2005 and atmosphere-land CO₂ flux for the decades of 1960s through 2000s is actually different. This is shown in Figure 4 where the 1850-2005 cumulative atmosphere-land CO₂ flux for both CanESM2 and CanESM4.2 ($\gamma_d = 0.40$) lies within the uncertainty range of -11 ± 47 PgC, but CanESM4.2 yields much better agreement with atmosphere-land CO₂ fluxes for the decades of 1960s through 2000s.

page 14, discussion on “relaxed CO₂” approach. This seems to be a side point that isn’t fully explained here, and I suggest either going into a bit more detail of what you mean (with figures or schematics) or else delete. Is the point that when you run it with relaxed CO₂, you are able to assess whether or the model is in equilibrium? Or is the point that the 3D structure and seasonal variation of the CO₂ matters from a radiative perspective and therefore leads to a different baseline climate than in the specified CO₂ case?

We have substantially revised section 2.2.3 to clarify the benefits of the “relaxed CO₂” approach.

table 1: It might be useful to add a row here with the purpose of each scenario.

This modification has been made.

figure 1: Why is this functional form of the downregulation factor chosen? Assuming that the downregulation is meant to capture progressive nutrient limitation, it doesn’t actually seem very progressive—the initial slope is quite high and then lessens at higher CO₂, but wouldn’t one expect a priori that nutrient limitations ought to become stronger only at higher CO₂ levels? Secondly, I can imagine that part of this phase space in this figure would be effectively excluded in that it would actually cause GPP to decrease under elevated CO₂, but it isn’t apparent from the figure where that boundary would occur. have you performed

C8

sufficient sensitivity studies to identify where that transition is? Thirdly, the minimal downregulation case is quite close to the standard model, why was that chosen?

Thank you for another good question. As explained in Arora et al. (2009), the functional form of the down-regulation factor derives from the fact that earlier simpler models of net or gross primary productivity (NPP or GPP) expressed it as a logarithmic function of atmospheric CO₂ concentration (e.g. Cao et al., 2001; Alexandrov and Oikawa, 2002).

$$G(t) = G_0 \left(1 + \gamma_p \ln \left(\frac{C(t)}{C_0} \right) \right) \quad (1)$$

where GPP at any given time, $G(t)$, is a function of its initial value G_0 , CO₂ concentration at time t , $C(t)$, and its initial value C_0 . The rate of increase of GPP is determined by the parameter γ_p .

The ratio of GPP in two different versions of a model in which they increase at different rates (γ_p and let's say γ_d) is given by

$$\frac{1 + \gamma_d \ln \frac{C(t)}{C_0}}{1 + \gamma_p \ln \frac{C(t)}{C_0}} \quad (2)$$

Equation (2) forms the basis for the functional form of down-regulation. For the case when $\gamma_d < \gamma_p$ the above ratio is less than 1 and its difference from 1 increases as $C(t)$ increase. In this sense the down-regulation is progressive. However, as reviewer # 3 notes the slope of down-regulation factor decreases. This second-order effect is a limitation of the formulation and we will make a note of this in revising our manuscript.

Reviewer # 3 raises a good point in regards to the boundary at which GPP may actually start to decrease with increasing CO₂. Although we have not derived the analytical equations that would allow to find where this boundary occurs, the model does not show any indication of decreasing GPP at least up until atmospheric CO₂ concentration of around 1000 ppm (as in the RCP 8.5 scenario) (see Arora and Boer, 2014). Although not relevant for this manuscript this comment provides us the reason to derive those analytical equations.

Finally, the values of γ_d chosen are equal to 0.40 ± 0.15 . While the minimal downregulation case ($\gamma_d = 0.55$) appears close to the standard model ($\gamma_d = 0.4$) in Figure 1 this isn't in the case for the results obtained (see e.g. Figures 4a, 5a, 5c, and 7) because of the non-linear

C9

behaviour of the system.

We have modified the manuscript to clarify these points.

page 28, last paragraph. Implicit in this argument seems to be the idea that the degree of historical growth and the response of the terrestrial biosphere over the historical period ought to be informative of an idealized 1%/yr forcing. But to the extent that downregulation is progressively driven by nutrient limitations, it ought to be expressed differently based on the rate at which CO₂ increases. So it may be just as informative to consider an extremely rapid CO₂ increase even if not at global scale, as in a FACE experiment, as it is to consider the slower-than 1%/yr forcing that has been applied globally over the historical period.

It wasn't our intent to imply that the 1% per year increasing CO₂ simulation is in any way indicative of the model response over the historical period, or vice-versa. The reference to Figure 2 again in this last paragraph of the manuscript was merely to mention that the value of $\gamma_d = 0.4$ that gives best comparison against observation-based determinants of the historical carbon budget makes CanESM4.2 an outlier amongst CMIP5 models. We now clarify this in the last paragraph of Section 5.0.

References

- Alexandrov, G., and T. Oikawa: TsuBiMo: a biosphere model of the CO₂ fertilization effect, 750 Clim. Res., 19, 265-270, 2002.
- Arora, V. K. and Boer, G. J.: Uncertainties in the 20th century carbon budget associated with land use change, Glob. Change Biol., 16, 3327–3348, 2010.
- Arora, V. K. and Boer, G. J.: A parameterization of leaf phenology for the terrestrial ecosystem component of climate models, Glob. Change Biol., 11, 39–59, doi:10.1111/j.1365-2486.2004.00890.x, 2005.
- Arora, V. K. and Boer, G. J.: Terrestrial ecosystems response to future changes in climate and atmospheric CO₂ concentration, Biogeosciences, 11, 4157-4171, doi:10.5194/bg-11-4157-2014, 2014.
- Arora, V. K., Boer, G. J., Christian, J. R., Curry, C. L., Denman, K. L., Zahariev, K., Flato, G. M., Scinocca, J. F., Merryfield, W. J., and Lee, W. G.: The effect of terrestrial photosynthesis down-regulation on the 20th century carbon budget simulated with the CCCma Earth System Model, J. Climate, 22, 6066–6088, 2009.
- Cao, M., Q. Zhang, and H.H. Shugart: Dynamic responses of African ecosystem carbon cycling to climate

change, *Clim. Res.*, 17, 183-193, 2001.

Garnaud, C., L. Sushama, V. K. Arora: The effect of driving climate data on the simulated terrestrial carbon pools and fluxes over North America, *International Journal of Climatology* 34 (4), 1098-1110, 2014.

Houghton, R. A.: Carbon flux to the atmosphere from land-use changes: 1850–2005, in: *TRENDS: a Compendium of Data on Global Change*, Carbon Dioxide Information Analysis Center, Oak Ridge National Laboratory, U.S. Department of Energy, Oak Ridge, Tenn., USA, 2008.

Le Quéré, C., Moriarty, R., Andrew, R. M., Peters, G. P., Ciais, P., Friedlingstein, P., Jones, S. D., Sitch, S., Tans, P., Arneeth, A., Boden, T. A., Bopp, L., Bozec, Y., Canadell, J. G., Chini, L. P., Chevallier, F., Cosca, C. E., Harris, I., Hoppema, M., Houghton, R. A., House, J. I., Jain, A. K., Johannessen, T., Kato, E., Keeling, R. F., Kitidis, V., Klein Goldewijk, K., Koven, C., Landa, C. S., Landschützer, P., Lenton, A., Lima, I. D., Marland, G., Mathis, J. T., Metz, N., Nojiri, Y., Olsen, A., Ono, T., Peng, S., Peters, W., Pfeil, B., Poulter, B., Raupach, M. R., Regnier, P., Rödenbeck, C., Saito, S., Salisbury, J. E., Schuster, U., Schwinger, J., Séférian, R., Segschneider, J., Steinhoff, T., Stocker, B. D., Sutton, A. J., Takahashi, T., Tilbrook, B., van der Werf, G. R., Viovy, N., Wang, Y.-P., Wanninkhof, R., Wiltshire, A., and Zeng, N.: Global carbon budget 2014, *Earth Syst. Sci. Data*, 7, 47–85, doi:10.5194/essd-7-47-2015, 2015.

Melton, J. R. and Arora, V. K.: Sub-grid scale representation of vegetation in global land surface schemes: implications for estimation of the terrestrial carbon sink, *Biogeosciences*, 11, 1021-1036, doi:10.5194/bg-11-1021-2014, 2014.

Melton, J. R., Shrestha, R. K., and Arora, V. K.: The influence of soils on heterotrophic respiration exerts a strong control on net ecosystem productivity in seasonally dry Amazonian forests, *Biogeosciences*, 12, 1151-1168, doi:10.5194/bg-12-1151-2015, 2015.

Peng, Y., Arora, V. K., Kurz, W. A., Hember, R. A., Hawkins, B. J., Fyfe, J. C., and Werner, A. T.: Climate and atmospheric drivers of historical terrestrial carbon uptake in the province of British Columbia, Canada, *Biogeosciences*, 11, 635-649, doi:10.5194/bg-11-635-2014, 2014.

Schimel, D., Stephens, B. B., and Fisher, J. B.: Effect of increasing CO₂ on the terrestrial carbon cycle, *Proceedings of the National Academy of Science U.S.A.*, 112, 436–441, doi:10.1073/pnas.1407302112, 2015.

Interactive comment on *Geosci. Model Dev. Discuss.*, doi:10.5194/gmd-2015-252, 2016.

1
2
3
4
5
6
7
8
9
10
11
12
13
14
15
16
17
18
19

On constraining the strength of the terrestrial CO₂ fertilization effect in an Earth system model

V. K. Arora and J. F. Scinocca.

Canadian Centre for Climate Modelling and Analysis, Environment and Climate Change Canada,
University of Victoria, Victoria, B.C., V8W 2Y2, Canada

Formatted: Space Before: 12 pt

20 **Abstract**

21

22 Earth system models (ESMs) explicitly simulate the interactions between the physical climate
23 system components and biogeochemical cycles. Physical and biogeochemical aspects of ESMs
24 are routinely compared against their observation-based counterparts to assess model performance
25 and to evaluate how this performance is affected by ongoing model development. Here, we assess
26 the performance of version 4.2 of the Canadian Earth system model against four, land carbon
27 cycle focused, observation-based determinants of the global carbon cycle and the historical global
28 carbon budget over the 1850-2005 period. Our objective is to constrain the strength of the
29 terrestrial CO₂ fertilization effect which is known to be the most uncertain of all carbon cycle
30 feedbacks. The observation-based determinants include 1) globally-averaged atmospheric CO₂
31 concentration, 2) cumulative atmosphere-land CO₂ flux, 3) atmosphere-land CO₂ flux for the
32 decades of 1960s, 1970s, 1980s, 1990s and 2000s and 4) the amplitude of the globally-averaged
33 annual CO₂ cycle and its increase over the 1980 to 2005 period. The optimal simulation that
34 satisfies constraints imposed by the first three determinants yields a net primary productivity
35 (NPP) increase from ~58 Pg C/yr in 1850 to about ~74 Pg C/yr in 2005; an increase of ~27% over
36 the 1850-2005 period. The simulated loss in the global soil carbon amount due to anthropogenic
37 land use change over the historical period is also broadly consistent with empirical estimates. Yet,
38 it remains possible that these determinants of the global carbon cycle are insufficient to
39 adequately constrain the historical carbon budget, and consequently the strength of terrestrial CO₂
40 fertilization effect as it is represented in the model, given the large uncertainty associated with
41 LUC emissions over the historical period.

42

43 **1. Introduction**

44

45 The evolution of the atmospheric CO₂ concentration in response to anthropogenic fossil fuel CO₂
46 emissions is determined by the rate at which a fraction of these emissions is taken up by the land
47 and ocean. Had the land and ocean not provided this “ecosystem service” since the start of the
48 industrial era, and not removed about 50% of CO₂ emissions from the atmosphere (Knorr, 2009),
49 the present concentration of CO₂ in the atmosphere would have been around 500 ppm, compared
50 to its current value of around 400 ppm. Over land, temperate and boreal forests as well as forests
51 in the tropical region are known to be sinks of atmospheric carbon (Ciais et al., 2013; Gourdji et
52 al., 2012; Schimel et al., 2015). The sink in the tropical forests is, however, compensated by
53 anthropogenic land use change emissions (Phillips and Lewis, 2014). Over ocean, the uptake of
54 anthropogenic carbon is observed to be larger in the high latitudes than in the tropical and
55 subtropical regions (Khatiwala et al., 2009). The manner in which the land and ocean will
56 continue to provide this ecosystem service in future is of both scientific and policy relevance.

57

58 Future projections of atmospheric CO₂ concentration, [CO₂], in response to continued
59 anthropogenic CO₂ emissions, or alternatively projections of CO₂ emissions compatible with a
60 given future [CO₂] pathway, are based primarily on comprehensive Earth system models (ESMs)
61 which include interactive land and ocean carbon cycle components (Jones et al., 2013). The land
62 and ocean carbon cycle components in ESMs respond both to increases in [CO₂] as well as the
63 associated changes in climate. These carbon components also respond to changes in climate
64 associated with other forcings including changes in concentration of non-CO₂ greenhouse gases
65 and aerosols, to nitrogen deposition and over land to anthropogenic land use change (LUC).

66

67 The response of land and ocean carbon cycle components to changes in [CO₂] and the associated
68 change in climate is most simply characterized in the framework of the 140-year long 1% per year
69 increasing CO₂ (1pctCO₂) experiment, in which [CO₂] increases at a rate of 1% per year from
70 pre-industrial value of about 285 ppm until concentration quadruples to about 1140 ppm. The
71 1pctCO₂ experiment has been recognized as a standard experiment by the coupled model
72 intercomparison project (CMIP) which serves to quantify the response of several climate and
73 Earth system metrics to increasing CO₂. These metrics include the transient climate response
74 (TCR) and the transient climate response to cumulative emissions (TCRE, Gillett et al., 2013).
75 Arora et al. (2013) analyzed results from fully-, biogeochemically- and radiatively-coupled
76 versions of the 1pctCO₂ experiment from eight ESMs that participated in the phase five of the
77 CMIP (CMIP5). They calculated the response of land and ocean carbon cycle components to
78 changes in [CO₂] and the associated change in climate expressed in terms of carbon-concentration
79 and carbon-climate feedbacks, respectively. Arora et al. (2013) found that of all the carbon cycle
80 feedbacks, the carbon-concentration feedback over land, which is primarily determined by the
81 strength of the terrestrial CO₂ fertilization effect, is the most uncertain across models. They found
82 that while the uncertainty in the carbon-concentration feedback over land (expressed in terms of
83 the standard deviation of the magnitude of the feedbacks) had somewhat reduced since the first
84 coupled carbon cycle climate model intercomparison project (C⁴MIP) (Friedlingstein et al., 2006)
85 its uncertainty remained the largest of all carbon cycle feedbacks. The comparison of the actual
86 magnitudes of the carbon cycle feedbacks over land is, however, not straightforward between the
87 Arora et al. (2013) and Friedlingstein et al. (2006) studies because they used different CO₂
88 scenarios.

Formatted: Subscript

90 The reason for this large uncertainty is that it is fairly difficult at present to constrain the strength
91 of the terrestrial CO₂ fertilization effect at the global scale. The net atmosphere-land CO₂ flux
92 since the start of the industrial era has not only been influenced by the changes in [CO₂] but also
93 the associated change in climate (due both to changes in [CO₂] and other climate forcers),
94 nitrogen deposition, and more importantly land use change - the contribution of which itself
95 remains highly uncertain. Since it is difficult to estimate the observed magnitude of net
96 atmosphere-land CO₂ flux since the start of the industrial era attributable only to increase in
97 [CO₂] it is consequently difficult to estimate the strength of the terrestrial CO₂ fertilization effect.

98

99 Measurements at Free-Air CO₂ Enrichment (FACE) sites in which vegetation is exposed to
100 elevated levels of [CO₂] help to assess some aspects of CO₂ fertilization and how nutrients
101 constraints regulate photosynthesis at elevated [CO₂] (Medlyn et al., 1999; McGuire et al., 1995).
102 However, FACE results cannot be easily extrapolated to the global scale and the response of
103 vegetation corresponds to a step increase in [CO₂] not the gradual increase which the real world
104 vegetation is experiencing.

105

106 As part of the ongoing evaluation of carbon cycle in ESMs, the model simulated aspects of the
107 global carbon cycle are routinely evaluated against their observation-based counterparts. These
108 evaluations also provide the opportunity to adjust physical processes that influence the strength of
109 the terrestrial CO₂ fertilization effect to provide the best comparison with observation-based
110 aspects of the global carbon cycle. Here, we present results from such an evaluation for a new
111 version of the Canadian Earth system model (CanESM4.2). An earlier version of the Canadian
112 Earth system model (CanESM2, Arora et al., 2011) participated in the CMIP5 (Taylor et al. 2012)

113 and its results also contributed to the fifth assessment report (AR5) of the Intergovernmental
114 Panel on Climate Change (IPCC). We evaluate the response of CanESM4.2, for three different
115 strengths of the terrestrial CO₂ fertilization effect, against four observation-based determinants of
116 the global carbon cycle and the historical global carbon budget over the 1850-2005 period, with a
117 focus on the land carbon cycle component. These determinants include 1) globally-averaged
118 atmospheric CO₂ concentration, 2) cumulative atmosphere-land CO₂ flux, 3) atmosphere-land
119 CO₂ flux for the decades of 1960s, 1970s, 1980s, 1990s and 2000s, and 4) the amplitude of the
120 globally-averaged annual CO₂ cycle and its increase over the 1980 to 2005 period.

121

122 The strength of the CO₂ fertilization effect influences all four of these determinants of the global
123 carbon cycle and the historical carbon budget. A stronger CO₂ fertilization effect, of course,
124 implies a larger carbon uptake by land and consequently a lower rate of increase of [CO₂] in
125 response to anthropogenic fossil fuel emissions. However, the strength of the CO₂ fertilization
126 effect also influences the amplitude of the annual [CO₂] cycle which is primarily controlled by the
127 northern hemisphere's biospheric activity. The amplitude of the annual [CO₂] cycle has been
128 observed to increase over the past five decades suggesting a gradual increase in photosynthesis in
129 association with a strengthening of the CO₂ fertilization effect (Keeling et al., 1996 ; Randerson et
130 al., 1997) and thus possibly can help to constrain the strength of the terrestrial CO₂ fertilization
131 effect in Earth system models.

132

133 **2. The coupled climate-carbon system and CanESM4.2**

134

135 **2.1 The coupled climate-carbon system**

136

137 The globally-averaged and vertically-integrated carbon budget for the combined atmosphere-
 138 land-ocean system may be written as:

$$139 \frac{dH_G}{dt} = \frac{dH_A}{dt} + \frac{dH_L}{dt} + \frac{dH_O}{dt} = E_F \quad (1)$$

141 where the Global carbon pool $H_G = H_A + H_L + H_O$ is the sum of carbon in the Atmosphere, Land
 142 and Ocean components, respectively (Pg C), and E_F is the rate of anthropogenic CO₂ emissions
 143 (Pg C/yr) into the atmosphere. The equations for the atmosphere, land and ocean components are
 144 written as

$$146 \begin{aligned} \frac{dH_A}{dt} &= F_A + E_F \\ &= -F_L - F_O + E_F \\ &= -(F_l - E_L) - F_O + E_F \\ &= -F_l - F_O + E_F + E_L \end{aligned} \quad (2)$$

$$147 \frac{dH_L}{dt} = F_L = F_l - E_L$$

$$\frac{dH_O}{dt} = F_O$$

148 where $(F_L + F_O) = -F_A$ are the fluxes (Pg C/yr) between the atmosphere and the underlying land
 149 and ocean, taken to be positive into the components. The net atmosphere-land CO₂ flux
 150 $F_L = F_l - E_L$ is composed of LUC emission rate E_L (Pg C/yr) as well as the remaining global
 151 “natural” CO₂ flux F_l that is often referred to as the residual or missing land sink in the context of
 152 the historical carbon budget (Le Quéré et al., 2015). The emissions associated with LUC occur
 153 when natural vegetation, for example, is deforested and replaced by croplands resulting in net loss
 154 of carbon from land to the atmosphere (i.e. positive E_L). Conversely, when croplands are
 155

156 abandoned and gradually replaced by forests then carbon is gained from atmosphere into the land
 157 (i.e. negative E_L).

158

159 Over land, the rate of change of carbon is reflected in the model's three land pools (vegetation, V ;
 160 soil, S ; and litter or detritus, D)

$$\begin{aligned}
 \frac{dH_L}{dt} &= F_L = F_i - E_L \\
 &= \frac{dH_V}{dt} + \frac{dH_S}{dt} + \frac{dH_D}{dt} \\
 &= (G - R_A) - R_H - E_L \\
 &= N - R_H - E_L
 \end{aligned}
 \tag{3}$$

162 where G is the gross primary productivity (Pg C/yr) which represents the rate of carbon uptake by
 163 vegetation through photosynthesis, and R_A and R_H are the autotrophic and heterotrophic
 164 respiratory fluxes (Pg C/yr) from living vegetation and dead litter and soil carbon pools,
 165 respectively. $N = G - R_A$ is the net primary productivity (NPP) which represents the carbon
 166 uptake by vegetation after autotrophic respiratory costs have been taken into account. The
 167 heterotrophic respiration $R_H = R_{H,D} + R_{H,S}$ is composed of respiration from the litter and soil
 168 carbon pools. The rate of change in carbon in model's litter (H_D) and soil (H_S) pools is written as

$$\begin{aligned}
 \frac{dH_D}{dt} &= D_L + D_S + D_R - C_{D \rightarrow S} - R_{H,D} \\
 \frac{dH_S}{dt} &= C_{D \rightarrow S} - R_{H,S}
 \end{aligned}
 \tag{4}$$

170 where $D_{i,i=L,S,R}$ is the litter fall from the model's *Leaf*, *Stem* and *Root* components into the
 171 model's litter pool. $C_{D \rightarrow S}$ is the transfer of humidified litter into the soil carbon pool calculated as
 172 a fraction of the litter respiration ($R_{H,D}$)

$$C_{D \rightarrow S} = \chi R_{H,D}
 \tag{5}$$

174 and χ is the humification factor.

175

176 Integrating (2) and (3) in time with $\int_{t_0}^t (dH/dt)dt = H(t) - H(t_0) = \Delta H(t)$ and $\int_{t_0}^t F dt = \tilde{F}(t)$ (Pg

177 C) gives

$$\begin{aligned}\Delta H_A &= -(\tilde{F}_O + \tilde{F}_I) + (\tilde{E}_F + \tilde{E}_L) \\ \Delta H_O &= \tilde{F}_O \\ \Delta H_L &= \tilde{F}_L = \tilde{F}_I - \tilde{E}_L; \\ &= \Delta H_V + \Delta H_S + \Delta H_D = \tilde{F}_I - \tilde{E}_L = \tilde{N} - \tilde{R}_H - \tilde{E}_L \\ \Delta H_I &= \tilde{F}_I \\ \Delta H &= \tilde{E}_F\end{aligned}\quad (6)$$

179 The cumulative change in the atmosphere, the ocean and the land carbon pools is written as

$$\begin{aligned}\Delta H_A + \Delta H_O + (\Delta H_I - \tilde{E}_L) &= \tilde{E}_F \\ \Delta H_A + \Delta H_O + \Delta H_I &= \tilde{E}_F + \tilde{E}_L = \tilde{E}\end{aligned}\quad (7)$$

181 where \tilde{E} (Pg C) is the cumulative sum of the anthropogenic emissions from fossil fuel
182 consumption and land use change. When emissions associated with LUC are zero, equation (7)

183 becomes

$$\Delta H_A + \Delta H_O + \Delta H_L = \tilde{E}_F = \tilde{E}\quad (8)$$

185 which indicates how cumulative emissions are parsed into changes in atmospheric carbon burden
186 and carbon uptake by the ocean and land components.

187

188 2.2 Canadian Earth System Model version 4.2

189

190 2.2.1 Physical components

191
192 At the Canadian Centre for Climate Modelling and Analysis (CCCma), the earth system model,
193 CanESM2, has undergone further development since its use for CMIP5. This version of the
194 model has been equivalently labelled CanESM4.0 in an effort to rationalize the ESM naming
195 convention to better reflect the fact that this model version employs the 4th generation atmosphere
196 component, CanAM4, (Von Salzen et al. 2013) and the 4th generation ocean component, CanOM4
197 (Arora et al., 2011). The version of the CCCma earth system model used for this study is
198 CanESM4.2 and so, represents two full cycles of model development on all of its components.
199 Similar to CanESM2, the physical ocean component of CanESM4.2 (CanOM4.2) has 40 levels
200 with approximately 10 m resolution in the upper ocean while the horizontal ocean resolution is
201 approximately 1.41° (longitude) \times 0.94° (latitude). The majority of development in CanESM4.2,
202 relative to CanESM2, has occurred on its atmospheric component CanAM4.2. CanAM4.2 is a
203 spectral model employing T63 triangular truncation with physical tendencies calculated on a 128
204 \times 64 ($\sim 2.81^\circ$) horizontal linear grid with 49 layers in the vertical whose thicknesses increase
205 monotonically with height to 1 hPa. Relative to CanAM4, CanAM4.2 includes a new version of
206 the Canadian Land Surface Scheme, CLASS3.6, which models the energy and water fluxes at the
207 atmosphere-land boundary by tracking energy and water through the soil, snow, and vegetation
208 canopy components (Verseghy, 2012). CLASS models the land surface energy and water balance
209 and calculates liquid and frozen soil moisture, and soil temperature for three soil layers (with
210 thicknesses 0.1, 0.25 and 3.75 m). The thickness of the third layer depends on the depth to
211 bedrock (and is in many places less than 3.75 m) based on the Zobler (1986) soil data set.
212 Changes to CLASS primarily include improvements to the simulation of snow at the land surface.
213 These incorporate new formulations for vegetation interception of snow (Bartlett et al., 2006), for

214 unloading of snow from vegetation (Hedstrom and Pomeroy, 1998), for the albedo of snow-
215 covered canopies (Bartlett and Verseghy, 2015), for limiting snow density as a function of depth
216 (Tabler et al., 1990; Brown et al., 2006), and for the thermal conductivity of snow (Sturm et al.,
217 1997). Water retention in snowpacks has also been incorporated. CanAM4.2 also includes an
218 aerosol microphysics scheme (von Salzen, 2006; Ma et al., 2008; Peng et al., 2012), a higher
219 vertical resolution in the upper troposphere, a reduced solar constant (1361W/m^2) and an
220 improved treatment of the solar continuum used in the radiative transfer. CanAM4.2 also
221 considers natural and anthropogenic aerosols and their emissions, transport, gas-phase and
222 aqueous-phase chemistry, and dry and wet deposition as summarized in Namazi et al. (2015)

223

224 **2.2.2 Land and ocean carbon cycle components**

225

226 The ocean and land carbon cycle components of CanESM4.2, are similar to CanESM2, and
227 represented by the Canadian Model of Ocean Carbon (CMOC) (Christian et al., 2010) and the
228 Canadian Terrestrial Ecosystem Model (CTEM) (Arora et al., 2009; Arora and Boer, 2010),
229 respectively.

230

231 LUC emissions in CTEM are modelled interactively on the basis of changes in land cover which
232 are determined by changes in crop area. The historical land cover used in the simulations
233 presented here is reconstructed using the linear approach of Arora and Boer (2010) and is the
234 same as used for CMIP5 simulations; as the fraction of crop area in a grid cell changes, the
235 fraction of non-crop plant functional types (PFTs) is adjusted linearly in proportion to their
236 existing coverage. The historical changes in crop area are based on the data set provided for

237 CMIP5 simulations as explained in Arora and Boer (2014). When the fraction of crop area in a
 238 grid cell increases then the fractional coverage of other PFTs is reduced which results in
 239 deforested biomass. The deforested biomass is allocated to three components that are i) burned
 240 instantaneously and contribute to ii) short (paper) and iii) long (wood products) term pools (Arora
 241 and Boer, 2010). The deforested biomass corresponding to paper and wood products is
 242 transferred to model's litter and soil carbon pools, respectively. When the fraction of crop area
 243 decreases, the fractional coverage of non-crop PFTs increases and their vegetation biomass is
 244 spread over a larger area reducing vegetation density. Carbon is sequestered until a new
 245 equilibrium is reached providing a carbon sink associated with regrowth as the abandoned areas
 246 revert back to natural vegetation.

247
 248 The LUC emissions term (E_L) in the equations (1) through (8) is not easily defined or calculated.
 249 Pongratz et al. (2014) discuss the multiple definitions and methods of calculating E_L . When E_L
 250 is calculated using models, it is most usually defined as the difference in F_L between simulations
 251 with and without LUC. This is also the basic definition used by Pongratz et al. (2014).
 252 Calculating E_L thus requires performing additional simulations without land use change in which
 253 land cover is held constant at its pre-industrial state. For a simulation without LUC equation (3)
 254 becomes

$$\frac{dH'_L}{dt} = F'_L = F'_I \quad (9)$$

256 and an estimate of E_L , and its cumulative values \tilde{E}_L , is obtained as

$$\begin{aligned} E_L &= F'_L - F_L \\ \tilde{E}_L &= \tilde{F}'_L - \tilde{F}_L \end{aligned} \quad (10)$$

258 Over the historical period, globally, F'_L is expected to be higher than F_L (both considered
259 positive downwards) due, at least, to two processes: 1) fraction of deforested biomass that is
260 burned and which contributes to short and long term product pools all release carbon to the
261 atmosphere, albeit at different time scales, 2) the area that is deforested and put under agricultural
262 use loses soil carbon and cannot sequester carbon in response to increase $[CO_2]$ since crops are
263 frequently harvested. As a result E_L is positive.

264

265 Relative to CanESM2, the version of CTEM employed in CanESM4.2, CTEM4.2, includes
266 changes to the humification factor (χ , see equations 4 and 5) which determines what fraction of
267 the humidified litter is transferred from litter (H_D) to the soil carbon pool (H_S). The value of χ
268 employed in CTEM4.2 has been changed for crop PFTs from 0.45 to 0.10, which decreases the
269 transfer of the humidified litter to the soil carbon ~~when natural vegetation is converted to~~
270 ~~croplands~~pool. As a result, a decrease in global soil carbon over the historical period is obtained
271 as natural vegetation is replaced by croplands as ~~would be expected based is seen in on~~
272 measurements (Wei et al., 2014). This change in humification factor was required despite the
273 higher litter decomposition rates over croplands and is discussed in more detail later in the results
274 section. In addition, in CTEM4.2 the sensitivity of photosynthesis to soil moisture is reduced for
275 coupling to CLASS 3.6, especially for the broadleaf evergreen PFT (which exists mainly in the
276 tropics) to somewhat account for deep roots, for example, in the Amazonian region (e.g. see da
277 Rocha et al., 2004).

278

279 CTEM has always included a parameterization of photosynthesis down-regulation, which
280 represents acclimatization to elevated CO_2 in the form of a decline in maximum photosynthetic

281 rate. In the absence of explicit coupling of terrestrial carbon and nitrogen cycles this
 282 parameterization yields a mechanism to reduce photosynthesis rates as [CO₂] increases. The
 283 photosynthesis down-regulation parameterization is described in detail in Arora et al. (2009). and
 284 is based on earlier simpler models which expressed net or gross primary productivity (NPP or
 285 GPP) as a logarithmic function of atmospheric CO₂ concentration (e.g. Cao et al., 2001;
 286 Alexandrov and Oikawa, 2002).

$$G(t) = G_0 \left(1 + \gamma_p \ln \left(\frac{C(t)}{C_0} \right) \right) \quad (11)$$

288 where GPP at any given time, $G(t)$, is a function of its initial value G_0 , atmospheric CO₂
 289 concentration at time t , $C(t)$, and its initial value C_0 . The rate of increase of GPP is determined by
 290 the parameter γ_p (where p indicates the “potential” rate of increase of GPP with CO₂). The ratio
 291 of GPP in two different versions of a model in which GPP increases at different rates (γ_p and γ_d)
 292 is given by

$$\xi(C) = \frac{1 + \gamma_d \ln(C/C_0)}{1 + \gamma_p \ln(C/C_0)} \quad (12)$$

295 where t is omitted for clarity. When $\gamma_d < \gamma_p$ — Briefly, the modelled “potential” gross
 296 photosynthesis rate (G_p), which is not constrained by nutrient limitation, can by is multiplied by a
 297 the scalar $\xi(C)$ (equation 142) which yields the gross primary productivity (G) used in equation
 298 (3) that now increases in response to CO₂ increases at a rate determined by the value of γ_d (the
 299 subscript d indicates down-regulation).

$$G = \xi(C) G_p \quad (143)$$

Formatted: Subscript

Formatted: Font: Italic

Formatted: Font: Italic

Formatted: Font: Italic

Formatted: Subscript

Formatted: Subscript

Formatted: Font: Italic

Formatted: Font: Italic

Formatted: Font: Italic

Formatted: Subscript

Formatted: Font: Italic

Formatted: Subscript

Formatted: Lowered by 16 pt

Formatted: Font: Italic

Formatted: Subscript

Formatted: Font: Italic

301
302 ~~where $\gamma_d < \gamma_p$.~~ A lower value of γ_d than γ_p yields a value of $\xi(C)$ that is less than one. As the
303 concentration of CO₂, expressed as C in equation (142), increases above its pre-industrial level C_0
304 (285 ppm), $\xi(C)$ progressively decreases resulting in a gross primary productivity G , which is
305 less than the its potential value G_p . Figure 1 shows the behaviour of $\xi(C)$ for $\gamma_p=0.95$ and three
306 values of γ_d (0.25, 0.4 and 0.55) corresponding to three different strengths of the terrestrial CO₂
307 fertilization effect. ~~The~~ A value of $\gamma_d = 0.25$ was used for CanESM2 to best simulate the globally-
308 averaged surface CO₂ concentration and cumulative 1850-2005 atmosphere-land CO₂ flux.
309 CanESM2, however, wasn't as rigorously evaluated as we have attempted here for CanESM4.2.
310 Through the parameter γ_d , the physical process of down-regulation has a direct influence on the
311 strength of the terrestrial CO₂ fertilization effect. In practice, different combinations of γ_d and γ_p
312 are able to yield very similar values of $\xi(C)$. Arora et al. (2009) calculated the value of γ_d based
313 on results from six studies, two of which were meta-analyses each based on 15 and 77 individual
314 studies, that grow plants in ambient and elevated CO₂ environment. Their results are equivalent to
315 $\gamma_d=0.46$ with a range from 0.22 to 0.63 for $\gamma_p=0.95$.

316
317 In Figure 1, while $\xi(C)$ decreases with an increase in atmospheric CO₂, indicating progressive
318 decline in photosynthesis due to nutrient limitation, the slope $\frac{d\xi}{dC}$ also decreases. Although a
319 second-order effect, this is a limitation of the current formulation of $\xi(C)$. A decreasing $\xi(C)$ as
320 CO₂ increases can eventually also lead to decrease in GPP although we have not seen this
321 behaviour up to CO₂ concentration of around 1000 ppm in simulations performed with CanESM2

Formatted: Subscript

Formatted: Subscript

Formatted: Font: 12 pt

Formatted: Subscript

Formatted: Lowered by 12 pt

Formatted: Subscript

Formatted: Subscript

322 (see Arora and Boer, 2014). While γ_d is used to model down-regulation of photosynthesis it may
323 also be used as a measure of the strength of the CO₂ fertilization effect. Lower values of γ_d
324 indicate higher down-regulation (see Figure 1) so higher values of γ_d imply higher strength of the
325 CO₂ fertilization effect. Finally, γ_d is specific to CTEM and as such the value of this parameter is
326 irrelevant to other models. More relevant for comparison with other models is the simulated rate
327 of increase of NPP over the historical period that a given value of γ_d yields.

Formatted: Subscript

Formatted: Subscript

329 **2.2.3 Treatment of CO₂ in the atmosphere**

330
331 The land and ocean components of the carbon cycle in CanESM4.2 are operable for two
332 experimental designs – 1) an ~~the~~ emissions-driven mode, where the atmospheric CO₂
333 concentration is a freely evolving 3D tracer in the model and 2) a concentrations-driven mode,
334 where the atmospheric CO₂ concentration is prescribed externally.

335
336 In the emissions-driven mode the anthropogenic CO₂ emissions (E_F) are specified and since the
337 interactive land and ocean carbon cycle components simulate the F_L and F_O terms, respectively,
338 the model is able to simulate the evolution of [CO₂] through the H_A term, which represents the
339 atmospheric carbon burden, in equation (2). This is referred to as the ~~“free” or~~ interactively
340 simulated [CO₂], or “free-CO2” configuration. In this case, the model simulates the transport of
341 CO₂ in the atmosphere ~~and as a result its producing~~ 3D structure, ~~in space, and its~~ annual cycle,
342 ~~through a year~~ and ~~its~~ inter-annual variability.

343

344 In the concentrations-driven mode, the land and ocean CO₂ fluxes, F_L and F_O , remain
345 interactively determined so model results can be used to diagnose the E_F term (based on equation
346 2) that is compatible with a given [CO₂] pathway at the global scale. The concentrations-driven
347 mode can be executed in two CanESM4.2 configurations. In the first configuration, a single scalar
348 value of [CO₂], which may be time evolving, is imposed at all geographical and vertical locations
349 in the model. This follows the CMIP5 prescription for concentrations-driven simulations and we
350 refer to it here as, “specified-CO₂” concentrations-driven mode. In the second configuration, a
351 new approach for specifying CO₂ concentration has been implemented in CanESM4.2. In this
352 new approach, only the globally averaged concentration of CO₂ in the lowest model level is
353 constrained by the prescribed value. The geographical and vertical distribution of CO₂ in the
354 atmosphere and its annual cycle in this second configuration is otherwise free to evolve in the
355 same manner as in ~~essentially identical to~~ the emissions-driven, free-CO₂ configuration, ~~mode~~
356 ~~except that it employs zero emissions and a strong relaxation on the global mean value of [CO₂]~~
357 ~~in the lowest model level towards the specified reference value.~~ A relaxation timescale of one
358 day is employed in this new -configuration and a fixed annual cycle, derived from the free-CO₂
359 preindustrial control simulation, is imposed on the reference value of [CO₂]. The reference value
360 of [CO₂] may additionally be specified as time-evolving ~~and includes a fixed annual cycle~~
361 ~~derived from the free CO₂ preindustrial control simulation.~~ We refer to this configuration as the
362 “relaxed-CO₂” concentrations-driven mode. Aside from the relaxational constraint on the global-
363 mean surface value of [CO₂], the atmospheric configuration for relaxed-CO₂ is identical to that
364 for free-CO₂ with zero emissions. As a consequence, the relaxed CO₂ configuration allows the
365 same nonlinearity in the atmosphere-surface exchange of CO₂ as the free CO₂ configuration
366 leading to nearly identical ~~The 3D structure and seasonal variation of CO₂ in the relaxed CO₂~~

Formatted: Not Superscript/ Subscript

Formatted: Not Superscript/ Subscript

367 case will have some radiative implications, compared to the specified CO₂ case, but the effects
368 are expected to be of second order since CO₂ is a fairly well mixed greenhouse gas. More
369 importantly, nonlinearity in the atmosphere-surface exchange of CO₂ means that the geographical
370 ~~structure and a seasonal cycle~~ of atmosphere CO₂ concentrations. In this
371 regard, the relaxed-CO₂ configuration is more physically more realistic than the specified-CO₂
372 configuration. The nonlinearity in the atmosphere-surface exchange of CO₂ means that the
373 geographical structure and a seasonal cycle allowed in the relaxed-CO₂ approach produces a
374 different, but more realistic, atmosphere-surface CO₂ exchange than the specified CO₂
375 configuration.

Formatted: Subscript

Formatted: Subscript

Formatted: Subscript

376 allowed in the relaxed CO₂ approach will produce a different atmosphere-surface CO₂ exchange
377 than the specified CO₂ configuration (the relaxed being much more similar to the free CO₂ case).

379 There are practical other advantages to using the relaxed-CO₂ configuration over the specified-
380 CO₂ configuration for concentrations-driven simulation experiments. When spinning up land
381 and ocean carbon pools for a prescribed atmospheric CO₂ concentration in the preindustrial
382 control simulation, the model is executed in concentrations driven mode to bring these pools into
383 equilibrium with a prescribed CO₂ concentration. In earlier versions of the CanESM, a specified-
384 CO₂ configuration was used for this purpose. Beginning with version 4.1, the relaxed-CO₂
385 configuration is used for this purpose because it produces little or no the equilibrated state of the
386 relaxed CO₂ configuration is found to produce little or no drift when used to initialize the free-
387 CO₂ preindustrial control simulations. In fact, the relaxed-CO₂ preindustrial control simulation
388 may be used as the control simulation for both emissions-driven and (relaxed-CO₂)

Formatted: Subscript

389 concentrations-driven experiments. This is not the case when the specified-CO₂ is used as the
390 configuration is employed for concentration driven experiments.

391

392 3. Experimental set up

393

394 Three different kinds of experiments are performed for this study. The first is the standard 1% per
395 year increasing CO₂ experiment (1pctCO₂) performed for three different strengths of the
396 terrestrial CO₂ fertilization effect. The 1pctCO₂ is a concentration-driven experiment and we use
397 the “relaxed-CO₂” configuration to specify CO₂ in the atmosphere. The second experiment is the
398 CMIP5 1850-2005 historical experiment, referred to as esmhistorical following CMIP5
399 terminology, which is performed with specified anthropogenic CO₂ emissions (i.e. in emissions-
400 driven, or “free-CO₂”, mode), where [CO₂] is simulated interactively. Concentrations of non-CO₂
401 greenhouse gases and emissions of aerosols and their precursors are specified in the esmhistorical
402 experiment following the CMIP5 protocol. The third experiment is same as the esmhistorical
403 experiment but LUC is not permitted and the land cover remains at its 1850 value; referred to as
404 the esmhistorical_noluc experiment. Two ensemble members are performed for each of the three
405 versions of the esmhistorical and esmhistorical_noluc experiments corresponding to three
406 different strengths of the terrestrial CO₂ fertilization effect. The rationale for performing historical
407 simulations without LUC is to be able to quantify LUC emissions E_L using equation (10). Table
408 1 summarizes all the simulations performed.

409

410 The 1pctCO₂ simulations with “relaxed” CO₂ for three different strengths of the terrestrial CO₂
411 fertilization effect are initialized from a corresponding pre-industrial control simulation with CO₂
412 specified at ~285 ppm and all other forcings at their 1850 values. The esmhistorical and

Formatted: Not Superscript/ Subscript

413 esmhistorical_noluc simulations are initialized from a pre-industrial control simulation with
414 “free” CO₂ and zero anthropogenic CO₂ emissions.

415

416 **4. Results**

417

418 **4.1. 1% per year increasing CO₂ experiments**

419

420 Figure 2 shows the carbon budget components of equation (8); ΔH_A , ΔH_O and ΔH_L i.e. the
421 change in atmospheric carbon burden and cumulative atmosphere-ocean and atmosphere-land
422 CO₂ flux which together make up the cumulative diagnosed emissions (\tilde{E}) based on results from
423 the fully-coupled 1pctCO2 experiment. Results are shown from eight CMIP5 models that
424 participated in the Arora et al. (2013) study, including CanESM2 which used $\gamma_d=0.25$, together
425 with those from CanESM4.2 for three different strengths of the terrestrial CO₂ fertilization effect.

426 The cumulative atmosphere-land CO₂ flux across models varies much more than the cumulative
427 atmosphere-ocean CO₂ flux across the CMIP5 models as already noted in Arora et al. (2013). The

428 results for CanESM4.2 indicate that the influence of γ_d (equation 1+2) on the strength of the
429 model’s terrestrial CO₂ fertilization effect allows CanESM4.2’s cumulative diagnosed emissions

430 to essentially span the range of the other CMIP5 models. For the three different strengths of the
431 terrestrial CO₂ fertilization effect, $\gamma_d = 0.25, 0.4$ and 0.55 , the γ_d values of 0.4 and 0.55 yield

432 cumulative atmosphere-land CO₂ flux that is higher than all the CMIP5 models. The basis for

433 choosing these values of γ_d within the range 0.4 ± 0.15 will become obvious later is that they span

434 the observation-based estimates of various quantities reasonably well as shown later.

435

436 The cumulative atmosphere-land CO₂ flux ΔH_L for CanESM4.2 for the simulation with $\gamma_d=0.25$
437 is higher than that for CanESM2 which also uses $\gamma_d=0.25$, because of the changes made to soil
438 moisture sensitivity of photosynthesis and because ΔH_L also depends on the model climate. In
439 particular, the CanESM2 bias of low precipitation over the Amazonian region has been reduced
440 in CanESM4.2, as shown in Figure 3. The increased precipitation over the Amazonian region
441 causes increased carbon uptake with increasing [CO₂]. The improved precipitation bias of
442 CanESM4.2 in this region is in part caused by the decreased sensitivity of photosynthesis to soil
443 moisture in CTEM4.2, especially for broadleaf evergreen PFT, which helps to increase
444 evapotranspiration and in turn increase precipitation over the region.

445

446 **4.2. Historical simulations with LUC**

447

448 The results presented in this section evaluate the model against four observation-based
449 determinants of the global carbon cycle and the historical global carbon budget over the 1850-
450 2005 period mentioned earlier. Simulated atmosphere-ocean CO₂ fluxes are also compared with
451 observation-based estimates although, of course, they are not directly affected by the strength of
452 the terrestrial CO₂ fertilization effect.

453

454 **4.2.1. Components of land carbon budget**

455

456 In Figure 4, time series of instantaneous (F_L panel a) and cumulative (\tilde{F}_L panel b) atmosphere-
457 land CO₂ flux over the period 1850-2005 are displayed for CanESM2 (which contributed results
458 to CMIP5) and CanESM4.2 for the three different strengths of the terrestrial CO₂ fertilization
459 effect. The observation-based estimates of $F_L = (F_i - E_L)$ in Figure 4a for the decades of 1960,

460 1970, 1980, 1990 and 2000 are reproduced from Le Quéré et al. (2015) who derive the
461 $F_L = (F_I - E_L)$ term as residual of the carbon budget equation $dH_A/dt = -(F_I - E_L) - F_O + E_F$
462 using observation-based estimates of change in atmospheric carbon budget (dH_A/dt),
463 atmosphere-ocean CO₂ flux (F_O) and fossil fuel emissions (E_F). The observation-based estimate
464 of -11 ± 47 Pg C in Figure 4b for \tilde{F}_L over the period 1850-2005 is from Arora et al. (2011) (their
465 Table 1).

466

467 The primary difference between CanESM2 and CanESM4.2 simulations in Figure 4 is that \tilde{F}_L for
468 CanESM2 generally stays positive throughout the historical period, whereas for CanESM4.2 it
469 first becomes negative (indicating that land is losing carbon) and then becomes positive
470 (indicating that land is gaining carbon) towards the end of the 20th century, depending on the
471 strength of the CO₂ fertilization effect. The behaviour of \tilde{F}_L for CanESM4.2 is considered to be
472 more realistic. As the land responds to anthropogenic land use change, associated with an increase
473 in crop area early in the historical period, it causes a decrease in vegetation and soil carbon (see
474 Figure 5). Later in the 20th Century, the CO₂ fertilization effect causes the land to become a sink
475 for carbon resulting in both vegetation and soil carbon increases. This behavior is consistent with
476 the mean model response of the 15 CMIP5 models analyzed by Hoffman et al. (2013) (their
477 Figure 2b). In contrast, CanESM2 shows a gradual increase in the global soil carbon amount
478 (Figure 5a) over the historical period. In Figure 5, it can be seen that the effect of CO₂ fertilization
479 in the second half of the 20th century is delayed for soil carbon compared to that for vegetation.
480 This is primarily because of the lag introduced by the turnover time of vegetation (i.e., increased
481 NPP inputs have to go through vegetation pool first) and the longer turnover time scale of the soil
482 carbon pool. The more reasonable response of soil carbon to anthropogenic land use change, in

483 Figure 5a for CanESM4.2, is achieved by changing the humification factor from 0.45 (in
484 CanESM2) to 0.10 (in CanESM4.2) in equation (5) which yields a reduction in global soil carbon
485 amount in response to land use change up until the time that the effect of CO₂ fertilization starts
486 to take effect. In Figure 4a, CanESM4.2 is also able to simulate continuously increasing F_L during
487 the period 1960 to 2005, depending on the strength of the CO₂ fertilization effect, while
488 CanESM2 simulates near constant or decreasing F_L from about 1990 onwards, as is also seen in
489 Figure 4b for \tilde{F}_L . This behaviour of F_L is not consistent with observation-based estimates from
490 Le Quéré et al. (2015) which show continued strengthening of the land carbon sink since 1960s.

491

492 In Figure 4a, amongst the three versions of the CanESM4.2, the simulation with $\gamma_d = 0.4$ (blue
493 line) yields the best comparison with observation-based estimates of F_L from Le Quéré et al.
494 (2015), while the simulations with $\gamma_d = 0.25$ (green line) and $\gamma_d = 0.55$ (red line) yield F_L values
495 that are lower and higher, respectively, than observation-based estimates. In Figure 4b, the
496 cumulative atmosphere-land CO₂ flux \tilde{F}_L over the 1850-2005 period from the simulations with
497 $\gamma_d = 0.25$ and 0.4 (green and blue lines, respectively) lies within the uncertainty of observation-
498 based estimates, while the simulation with $\gamma_d = 0.55$ (red line) yields \tilde{F}_L value that is high
499 relative to observation-based estimate.

500

501 Figure 6 shows the change in and absolute values of NPP from CanESM2 and the simulations
502 made with CanESM4.2 for three different strengths of the CO₂ fertilization effect. Consistent with
503 1pctCO2 simulations, the rate of increase of NPP in CanESM4.2 with $\gamma_d = 0.25$ is higher than
504 that in CanESM2 which also uses $\gamma_d = 0.25$. This is because the underlying model climate is

505 different in CanESM2 and CanESM4.2, as mentioned earlier, and the fact that photosynthesis
506 sensitivity to soil moisture has also been reduced. The rates of increase of NPP for $\gamma_d = 0.40$ and
507 0.50 are, of course, even higher. The CanESM4.2 simulation with $\gamma_d = 0.40$, which yields the
508 best comparison with observation-based estimates of F_L for the decade of 1960 through 2000
509 (Figure 4a) as well as \tilde{F}_L for the period 1850-2005 (Figure 4b), yields an increase in NPP of ~16
510 Pg C/yr over the 1850-2005 period. A caveat here is that part of this increase is also caused by
511 increase in the crop area over the historical period that is realized in the model regardless of the
512 strength of the CO₂ fertilization effect. In CTEM4.2, the maximum photosynthetic capacity of
513 crops is higher than for other PFTs to account for the fact that agricultural areas are generally
514 fertilized. As a result, increase in crop area also increases global NPP. The increasing crop
515 productivity has been suggested to contribute to the increase in amplitude of the annual [CO₂]
516 cycle since 1960s (Zeng et al., 2014). However, in the absence of an explicit representation of
517 terrestrial N cycle (and thus fertilization of cropped areas) or a representation of increase in crop
518 yield per unit area due to genetic modifications, the only processes in CTEM that contribute to
519 changes in crop yield are the change in crop area itself and the increase in crop NPP due to the
520 CO₂ fertilization effect.

521

522 **4.2.2. Globally-averaged [CO₂]**

523

524 Figure 7 shows the simulated globally-averaged surface [CO₂] from the emissions-driven
525 esmhistorical simulation of CanESM2 and that of CanESM4.2 for three different strengths of the
526 CO₂ fertilization effect. The observation-based time series of [CO₂] is illustrated by the heavy
527 black line. The CanESM2 ($\gamma_d=0.25$) simulation yields a reasonable comparison with observation-

528 based $[\text{CO}_2]$. Amongst the versions of CanESM4.2 with different strengths of the CO_2
529 fertilization effect, the version with $\gamma_d=0.40$ yield the best comparison. The CanESM4.2 version
530 with $\gamma_d=0.25$ (weaker strength of the CO_2 fertilization effect) and 0.55 (stronger CO_2 fertilization
531 effect) yield CO_2 concentrations that are respectively higher and lower than the observational
532 estimate from roughly mid-20th Century onward. The reason CanESM4.2 ($\gamma_d=0.40$) requires a
533 stronger CO_2 fertilization effect than CanESM2 ($\gamma_d=0.25$) for simulating the observation-based
534 increase in atmospheric CO_2 burden over the historical period is the enhanced impact of LUC in
535 CanESM4.2 due to its increased humification factor and the associated response of the global soil
536 carbon pool, as discussed in the previous section. The differences in simulated $[\text{CO}_2]$ in Figure 7
537 from CanESM4.2 are due only to differences in the strength of the CO_2 fertilization effect.
538 Although, of course, since in these simulations $[\text{CO}_2]$ is simulated interactively, the simulated
539 atmosphere-land flux F_L and $[\text{CO}_2]$ both respond to and affect each other.

540

541 Both CanESM2 and CanESM4.2 under-predict $[\text{CO}_2]$ relative to observational estimates over the
542 period 1850-1930, and are also unable to reproduce the near zero rate of increase of $[\text{CO}_2]$ around
543 1940. Possible reasons for these discrepancies include 1) the possibility that carbon cycle before
544 1850 was not in true equilibrium and this aspect cannot be captured since the model is spun up to
545 equilibrium for 1850 conditions, 2) the uncertainties associated with anthropogenic emissions for
546 the late 19th and early 20th century that are used to drive the model, and 3) the uncertainties
547 associated with pre Mauna-Loa $[\text{CO}_2]$ observations.

548

549 **4.2.3. Atmosphere-ocean CO_2 flux**

550

551 | Figures 8a and b, respectively, show time series of instantaneous (F_o) and cumulative (\tilde{F}_o)
552 | atmosphere-ocean CO₂ fluxes over the period 1850-2005 for the set of emissions-driven
553 | simulations presented in Fig. 7. The strength of the terrestrial CO₂ fertilization effect has little or
554 | no impact on the ocean biogeochemical processes. The differences in values of F_o and \tilde{F}_o for
555 | the three versions CanESM4.2 are, therefore, primarily due to the differences in [CO₂]. The
556 | observation-based estimates of F_o in Figure 8a for the decades of 1960, 1970, 1980, 1990 and
557 | 2000 are from Le Quéré et al. (2015). The observation-based estimate of \tilde{F}_o of 141 ± 27 Pg C in
558 | Figure 8b for the period 1850-2005 is from Arora et al. (2011) (their Table 1).

559

560 | Both CanESM2 and the CanESM4.2 simulation for $\gamma_d=0.40$ (which provides the best comparison
561 | with observation-based estimate for [CO₂]; blue line in Figure 7) yield lower \tilde{F}_o compared to
562 | observation-based values. The F_o value from CanESM2 and the CanESM4.2 simulation for
563 | $\gamma_d=0.40$ are lower than the mean estimates from Le Quéré et al. (2015) for the decades of 1960s
564 | through 2000s, although still within their uncertainty range. The family of ESMs from CCCma,
565 | all of which have the same physical ocean model, including CanESM1 (Arora et al., 2009),
566 | CanESM2 (Arora et al., 2011) and now CanESM4.2, yield lower than observed ocean carbon
567 | uptake over the historical period. Recent analyses of these model versions suggest that the
568 | primary reason for their low carbon uptake is a negative bias in near surface wind speeds over the
569 | Southern Ocean and an iron limitation in the same region which is too strong (personal
570 | communication, Dr. Neil Swart, Canadian Centre for Climate Modelling and Analysis). The
571 | CanESM4.2 simulation with $\gamma_d=0.25$ (green line in Figure 8) yields a better comparison with

572 observation-based estimates of F_o and \tilde{F}_o but that is because of the higher simulated $[\text{CO}_2]$ in
573 that simulation associated with lower carbon uptake by land.

574

575 **4.2.4. Amplitude of the annual CO_2 cycle**

576

577 The annual CO_2 cycle is influenced strongly by the terrestrial biospheric activity of the northern
578 hemisphere (Keeling et al., 1996; Randerson et al., 1997). Higher than normal biospheric uptake
579 of carbon during a northern hemisphere's growing season, for example, will yield lower than
580 normal $[\text{CO}_2]$ by the end of the growing season, around September when $[\text{CO}_2]$ is at its lowest
581 level (see Figure 9a). Similarly, during the northern hemisphere's dormant season, increased
582 respiration from live vegetation and decomposition of dead carbon, including leaf litter, that may
583 be associated with increased carbon uptake during the last growing season, will yield higher than
584 normal $[\text{CO}_2]$ during April when $[\text{CO}_2]$ is at its highest level. Both processes increase the
585 amplitude of the annual $[\text{CO}_2]$ cycle. Given this strong control, the rate of change of the
586 amplitude of the annual $[\text{CO}_2]$ cycle can potentially help to constrain the strength of the terrestrial
587 CO_2 fertilization effect.

588

589 Figure 9a compares the annual cycle of the trend-adjusted globally-averaged near-surface
590 monthly $[\text{CO}_2]$ anomalies from CanESM2 and the versions of CanESM4.2 for three different
591 strengths of the CO_2 fertilization effect with observation-based estimates for the 1991-2000
592 period. Figure 9b shows the time series of the amplitude of the annual cycle of the trend adjusted
593 globally-averaged near-surface monthly $[\text{CO}_2]$ anomalies (referred to as Φ_{CO_2}) from CanESM2
594 and CanEM4.2, as well as observation-based estimates going back to 1980s. While CO_2

595 measurements at Mauna Loa started in 1959, observation-based globally-averaged near-surface
596 [CO₂] values are only available since 1980s
597 (ftp://aftp.cmdl.noaa.gov/products/trends/co2/co2_mm_gl.txt). In Figure 9b, consistent with the
598 strengthening of the CO₂ fertilization effect, associated with the increase in [CO₂], the
599 observation-based estimate of Φ_{CO_2} shows an increase from 1980s to the present. Both CanESM2
600 and versions of CanESM4.2 also show an increase in the amplitude of Φ_{CO_2} over the period
601 1850-2005. However, the absolute values of Φ_{CO_2} are lower in CanESM2 than in CanESM4.2
602 (Figure 9b). Of course, in the absence of an observation-based estimate of pre-industrial value of
603 Φ_{CO_2} it is difficult to say which value is more correct. However, when considering the present
604 day values of Φ_{CO_2} the three versions of CanESM4.2 yield better comparison with observation-
605 based estimate as also shown in Figure 9a. The increase in the value of Φ_{CO_2} from CanESM2 to
606 CanESM4.2, which now yields better comparison with observation-based value of Φ_{CO_2} , is most
607 likely caused by the change in the land surface scheme from CLASS 2.7 (that is implemented in
608 CanESM2) to CLASS 3.6 (implemented in CanESM4.2), since the atmospheric component of the
609 model hasn't changed substantially. It is, however, difficult to attribute the cause of this
610 improvement in the present day value of Φ_{CO_2} in CanESM4.2 to a particular aspect of the new
611 version of the land surface scheme. The annual [CO₂] cycle is driven primarily by the response of
612 the terrestrial biosphere to the annual cycle of temperature and the associated greening of the
613 biosphere every summer in the northern hemisphere. However, the simulated amplitude of the
614 annual cycle of near-surface temperature hasn't changed substantially from CanESM2 to
615 CanESM4.2 (not shown).

616

617 In Figure 9b, the simulated values of Φ_{CO_2} for the CanESM4.2 simulations with $\gamma_d=0.25, 0.40$
618 and 0.55 are 4.41, 4.69 and 4.85 ppm, respectively, averaged over the period 1991-2000,
619 compared to observation-based value of Φ_{CO_2} of 4.36 ppm. Here, CanESM4.2 simulation with
620 $\gamma_d=0.25$ yields the best comparison with observation-based value of Φ_{CO_2} . An increase in the
621 strength of the CO_2 fertilization effect increases the amplitude of the annual $[CO_2]$ cycle so a
622 larger value of γ_d yields a larger value of Φ_{CO_2} . The increase in the amplitude of the annual
623 $[CO_2]$ cycle comes both from lower $[CO_2]$ at the end of the growing season in September as well
624 as higher $[CO_2]$ at the start of the northern hemisphere's growing season in April (see Figure 9a),
625 as mentioned earlier in this section.

626

627 More important than the absolute value of Φ_{CO_2} is its rate of increase over time which is a
628 measure of the strength of the terrestrial CO_2 fertilization effect. Figure 9b also shows the trend in
629 Φ_{CO_2} over the 1980-2005 overlapping period for which for both the model and observation-based
630 estimates of Φ_{CO_2} are available. The magnitude of trend for observation-based estimate of Φ_{CO_2}
631 is 0.142 ± 0.08 ppm/10-years (mean \pm standard deviation, $\bar{x} \pm \sigma_x$), implying that over the 26 year
632 1980-2005 period the amplitude of annual $[CO_2]$ cycle has increased by 0.37 ± 0.21 ppm. The
633 calculated mean and standard deviation of the observation-based trend, however, does not take
634 into account the uncertainty associated with the observation-based estimates of $[CO_2]$,
635 consideration of which will increase the calculated standard deviation even more. The magnitudes
636 of trend in Φ_{CO_2} simulated by CanESM2 ($\gamma_d=0.25$) and CanESM4.2 (for $\gamma_d=0.25$) are
637 0.103 ± 0.05 and 0.153 ± 0.031 , respectively, and statistically not different from the trend in the
638 observation-based value of Φ_{CO_2} implying an increase of 0.27 ± 0.13 and 0.40 ± 0.08 ppm,

639 respectively, in Φ_{CO_2} over the 1980-2005 period. The statistical difference is calculated on the
640 basis of $\bar{x} \pm 1.385 \sigma_x$ range which corresponds to 83.4% confidence intervals; the estimates from
641 two sources are statistically not different at the 95% confidence level if this range overlaps (Knol
642 et al., 2011). The magnitudes of the trend in Φ_{CO_2} over the 1980-2005 period for CanESM4.2
643 simulations with $\gamma_d = 0.4$ and 0.55 (0.328 ± 0.038 and 0.314 ± 0.034 ppm/10-years, respectively)
644 are, however, more than twice, and statistically different from the observation-based estimate
645 (0.142 ± 0.08 ppm/10-years).

646

647 Overall, the CanESM4.2 simulation with $\gamma_d=0.25$ yields the amplitude of the globally-average
648 annual CO_2 cycle and its rate of increase over the 1980-2005 period that compares best with
649 observation-based estimates.

650

651 **4.3. Historical simulations without LUC**

652

653 Figure 10 and 11 show results from CanESM4.2 emissions-driven simulations for three different
654 strengths of the CO_2 fertilization effect that do not implement anthropogenic LUC over the
655 historical period and compare them to their corresponding simulations with LUC.

656

657 Figure 10a compares the simulated $[CO_2]$; as expected in the absence of anthropogenic LUC the
658 simulated $[CO_2]$ is lower since LUC emissions do not contribute to increase in $[CO_2]$. The
659 difference in $[CO_2]$ at the end of the simulation, in year 2005, between simulations with and
660 without LUC is 29.0, 23.6 and 19.0 ppm for $\gamma_d=0.25$, 0.40 and 0.55. The simulations with the
661 lowest strength of the CO_2 fertilization effect ($\gamma_d=0.25$) yield the largest difference because these

662 simulations also have the largest [CO₂] amongst their set of simulations with and without LUC.
663 The CO₂ fertilization of the terrestrial biosphere implies that the effect of deforestation will be
664 higher, because of reduced carbon uptake by deforested vegetation, if background [CO₂] is
665 higher.

666

667 Figure 10b compares the simulated NPP from CanESM4.2 simulations with and without LUC.
668 The increase in simulated NPP, regardless of the strength of the CO₂ fertilization effect, is lower
669 over the historical period in simulations without LUC for two apparent reasons. First, the rate of
670 increase of [CO₂] is itself lower and second, in the absence of LUC, there is no contribution from
671 increasing crop area to NPP. Overall, the increase in NPP over the 1850-2005 period in
672 simulations with LUC is a little more than twice that in simulations without LUC. Figure 10c and
673 10d compare the changes in global vegetation biomass and soil carbon mass, over the historical
674 period, from simulations with and without LUC. As expected, in the absence of LUC, global
675 vegetation biomass and soil carbon mass more or less show a continuous increase, associated with
676 the increase in NPP which itself is due to the increase in [CO₂]. Consequently, in Figure 11a, the
677 cumulative atmosphere-land CO₂ flux \tilde{F}_L in simulations without LUC also shows a more or less
678 continuous increase over the historical period.

679

680 Finally, Figure 11b shows the diagnosed cumulative LUC emissions \tilde{E}_L calculated as the
681 difference between cumulative \tilde{F}_L , following equation 10, from simulations with and without
682 LUC. The ~~calculated~~ diagnosed \tilde{E}_L in this manner are equal to 95, 81 and 67 Pg C, over the 1850-
683 2005 period, for $\gamma_d=0.25, 0.40$ and 0.55 . The calculated diagnosed \tilde{E}_L are highest for $\gamma_d=0.25$

684 associated with the highest background simulated [CO₂] in these simulations, as mentioned
685 earlier. For comparison, LUC emissions estimated by Houghton (2008) for the period 1850-2005,
686 based on a book-keeping approach, are 156 Pg C but these estimates are generally believed to be
687 ±50% uncertain (see Figure 1 of Ramankutty et al. (2007)). LUC emissions, when calculated by
688 differencing F_L from simulations with and without LUC, also depend on the type of simulations
689 performed - in particular, if simulations are driven with specified CO₂ concentrations or specified
690 CO₂ emissions. Had our simulations been concentration-driven, in contrast to being emissions
691 driven, then both with and without LUC simulations would have experienced the same specified
692 observed CO₂ concentration over the historical period and the simulated LUC emissions would
693 have been higher. Arora and Boer (2010) found that diagnosed LUC emissions in the first version
694 of the Canadian Earth System Model (CanESM1) increased from 71 Pg C (for emissions-driven
695 simulations) to 124 Pg C (for concentration-driven simulations). Concentration-driven
696 simulations, however, cannot be evaluated against observation-based amplitude of the annual CO₂
697 cycle and its increase over the historical period. These simulations either ignore the annual cycle
698 of CO₂ (our specified-CO₂ case) or use a specified amplitude of the CO₂ annual cycle (our
699 relaxed-CO₂ case).

Formatted: Subscript

Formatted: Subscript

Formatted: Subscript

Formatted: Subscript

Formatted: Font: Not Bold

Formatted: Font: Not Bold, Subscript

Formatted: Font: Not Bold

Formatted: Font: Not Bold

Formatted: Font: Not Bold, Subscript

Formatted: Font: Not Bold

Formatted: Font: Not Bold

701 **5.0. Discussion and conclusions**

702

703 This study evaluates the ability of four observation-based determinants of the global carbon cycle
704 and the historical carbon budget to constrain the parameterization of photosynthesis down-
705 regulation, which directly determines the strength of the CO₂ fertilization effect, over the
706 historical period 1850-2005. The key parameter that controls ~~photosynthesis down-regulation the~~

707 strength of the CO₂ fertilization effect in CTEM, γ_d , was varied in the latest version of CCCma's
708 earth system model CanESM4.2. Comparing simulated and observation-based estimates of 1)
709 globally-averaged atmospheric CO₂ concentration, 2) cumulative atmosphere-land CO₂ flux, and
710 3) atmosphere-land CO₂ flux for the decades of 1960s, 1970s, 1980s, 1990s and 2000s, it is found
711 that the CanESM4.2 version with $\gamma_d=0.40$ yields the best comparison.

712
713 The evaluation of CTEM within the framework of CanESM4.2 presented here is based on an
714 emergent model property at the global scale and may be considered as a top-down approach of
715 model evaluation. In contrast, the bottom-up approaches of model evaluation typically evaluate
716 model results and processes against observations of primary atmosphere-land carbon and/or
717 nitrogen fluxes and sizes of the vegetation, litter and soil carbon/nitrogen pools (e.g. Zaehle et
718 al., 2014). Indeed, CTEM has been evaluated at point (e.g. Arora and Boer, 2005; Melton et al.,
719 2015), regional (e.g. Peng et al., 2014; Garnaud et al., 2014) and global (e.g. Arora and Boer,
720 2010; Melton and Arora, 2014) scales in a number of studies when driven with observation-based
721 reanalysis data. Both top-down and bottom-up approaches of model evaluation are complimentary
722 to each other and allow to evaluate different aspects of the model at different spatial and temporal
723 scales.

724
725 For the top-down approach used here, CanESM4.2 simulates globally-averaged near-surface
726 [CO₂] of 400, **381** and 368 ppm for $\gamma_d=0.25$, **0.40** and 0.55, respectively, compared to the
727 observation-based estimate of **379** ppm for year 2005. The cumulative atmosphere-land CO₂ flux
728 of 18 Pg C for the period 1850-2005 for $\gamma_d=0.40$ lies within the range of the observation-based
729 estimate of -11 ± 47 Pg C in Figure 4b, and so do the average atmosphere-land CO₂ flux for the

730 decades of 1960s through to 2000s in Figure 4a when compared to observation-based estimates
731 from Le Quéré et al. (2015). $\gamma_d=0.25$ and 0.55 yield average atmosphere-land CO_2 flux for the
732 decades of 1960s through to 2000s that are lower and higher, respectively, than the observation-
733 based estimates from Le Quéré et al. (2015). The only determinant against which $\gamma_d=0.40$ does
734 not yield the best comparison with observation-based estimates is the amplitude of the globally-
735 averaged annual CO_2 cycle and its increase over the 1980 to 2005 period. For this determinant,
736 $\gamma_d=0.25$ seems to yield the best comparison (Figure 9). The value of $\gamma_d=0.40$ that yields best
737 overall comparison with observation-based determinants of the global carbon cycle and the
738 historical carbon budget is also broadly consistent with Arora et al. (2009) who derived a value of
739 $\gamma_d=0.46$ based on results from FACE studies (as mentioned in Section 2.2.2).

740

741 The caveat with the analyses presented here, or for any model for that matter, is that the strength
742 of the terrestrial CO_2 fertilization effect is dependent on the processes included in the model and
743 the parameter values associated with them. The primary example of this is the adjustment to the
744 humification factor in CTEM4.2, which leads to reduction in the global soil carbon amount as
745 anthropogenic LUC becomes significant towards the mid-20th Century. This response of soil
746 carbon was not present in the model's configuration of CTEM and historical simulations made
747 with CanESM2. The representation of soil carbon loss, in response to anthropogenic LUC in
748 CanESM4.2, implies that a stronger CO_2 fertilization effect (or weaker photosynthesis down-
749 regulation) should be required to reproduce realistic atmosphere-land CO_2 flux over the historical
750 period and this was found to be the case in Figure 4a. Despite this dependence on processes
751 included in the model, the response of the land carbon cycle, over the historical period, to the two
752 primary forcings of increased $[\text{CO}_2]$ and anthropogenic land use change must be sufficiently

753 realistic in the model to satisfy all the four determinants of the global carbon cycle and the
754 historical global carbon budget.

755

756 The simulated loss in soil carbon in response to anthropogenic LUC over the historical period
757 may also be assessed against observation-based estimates from Wei et al. (2014). Using data from
758 453 sites that were converted from forest to agricultural land, Wei et al. (2014) find that the soil
759 organic carbon stocks decreased by an average of $43.1 \pm 1.1\%$ for all sites. Based on the HYDE
760 v3.1 data set from which the changes in crop area are derived (Hurtt et al., 2011), LUC as
761 implemented in CanESM4.2 yields an increase in crop area from about 5 million km² in 1850 to
762 about 15 million km² in 2005. Assuming an initial soil carbon amount of 10 Kg C/m² (see Figure
763 2c of Melton and Arora (2014)) and an average 40% decrease in soil carbon amount, based on
764 Wei et al. (2014), implies that the increase in crop area of about 10 million km² over the historical
765 period has likely yielded a global soil organic carbon loss of 40 Pg C. The loss in soil carbon in
766 Figure 5a is simulated to 18 Pg C for CanESM4.2 simulation with $\gamma_d = 0.40$, the simulation that
767 yield best comparison with observation-based determinants of the global carbon cycle and the
768 historical carbon budget. This loss of 18 Pg C is expected to be less than the 40 Pg C because the
769 model estimates also include an increase associated with the increase in NPP due to the CO₂
770 fertilization effect from non-crop areas. The effect of LUC on global soil carbon loss may also be
771 estimated by differencing global soil carbon amounts from simulations with and without LUC
772 from Figure 10d at the end of the simulation in year 2005. For CanESM4.2 simulation with $\gamma_d =$
773 0.40, this amounts to around 50 Pg C. Both these estimates of soil carbon loss are broadly
774 consistent with the back-of-the-envelope calculation of 40 Pg C soil carbon loss, based on Wei et

775 al. (2014) estimates, indicating that the soil carbon loss simulated in response to anthropogenic
776 LUC over the historical period is not grossly over or underestimated.

777

778 The CanESM4.2 simulation with $\gamma_d=0.40$, however, fails to satisfy the rate of increase of the
779 amplitude of the globally-averaged annual CO₂ cycle over the 1980-2005 period implying that
780 there are still limitations in the model structure and/or parameter values. Of course, the fact that
781 the amplitude of the globally-averaged annual CO₂ cycle is also affected by the atmosphere-ocean
782 CO₂ fluxes makes it more difficult to attribute the changes in the amplitude of the globally-
783 averaged annual CO₂ cycle solely to atmosphere-land CO₂ fluxes. Additionally, the increase in
784 crop area as well as crop yield per unit area over the historical period have been suggested by
785 Zeng et al. (2014) to contribute towards the observed increase in the amplitude of annual CO₂
786 cycle. Based on their sensitivity tests, Zeng et al. (2014) attribute 45, 29 and 26 percent of the
787 observed increase in the seasonal-cycle amplitude of the CO₂ cycle to LUC, climate variability
788 and change (including factors such as the lengthening of the growing season) and increased
789 productivity due to CO₂ fertilization, respectively. Comparison of the rate of increase of NPP in
790 CanESM4.2 experiments with and without LUC (Figure 10b), as a measure of increase in the
791 strength of the CO₂ fertilization effect, suggests that the contribution of anthropogenic LUC to the
792 increase in the seasonal-cycle amplitude is 52%, which is broadly consistent with the 45% value
793 obtained by Zeng et al. (2014).

794

795 While CanESM4.2 simulation with $\gamma_d=0.40$ is able to simulate a realistic rate of increase of
796 [CO₂] over the period 1960 to 2005, the modelled atmosphere-ocean CO₂ fluxes for this and the
797 CanESM2 version are lower than observational estimates of this quantity (Figure 8). This implies

798 that if the modelled atmosphere-ocean CO₂ flux were to increase and become more consistent
799 with observation-based estimates then the modelled atmosphere-land CO₂ flux must decrease to
800 still be able to yield sufficiently realistic rate of increase of [CO₂]. This implies that the strength
801 of the terrestrial CO₂ fertilization effect should likely be somewhat lower than what is obtained by
802 $\gamma_d=0.40$ or the simulated atmosphere-land CO₂ flux is higher because of some other reason, most
803 likely lower LUC emissions. Indeed, the required decrease in modelled atmosphere-land CO₂ flux
804 is consistent with the fact that the modelled LUC emissions for $\gamma_d=0.40$ (81 Pg C) are about half
805 the estimate from Houghton (2008) (156 Pg C) with the caveat, of course, that Houghton's
806 estimates themselves have an uncertainty of roughly $\pm 50\%$. The LUC module of CTEM currently
807 only accounts for changes in crop area and does not take into account changes associated with
808 pasture area given their ambiguous definition (pasture may or may not be grasslands). The model
809 also does not take into account wood harvesting which amongst other uses is also used as a
810 biofuel. Treatment of these additional processes will increase modelled LUC emissions.

811
812 Although the CanESM4.2 simulation with $\gamma_d=0.40$ satisfies three out of four constraints placed
813 by the chosen determinants of the global carbon cycle and the historical carbon budget, and also
814 simulates reasonable soil carbon loss in response to anthropogenic LUC, the model now yields
815 the highest land carbon uptake, in the ~~1pctCO2~~1pctCO2 experiment, amongst the CMIP5 models
816 that were compared by Arora et al. (2013) as seen in Figure 2. Of course, the 1pctCO2 experiment
817 is in no way indicative of models' performance over the historical period, nor is being an outlier
818 amongst CMIP5 models a conclusive evaluation of CanESM4.2's land carbon uptake. However,
819 it remains ~~It is quite~~ possible that the chosen determinants of the global carbon cycle and the
820 historical carbon budget are not able to constrain the model sufficiently, given the especially large

821 uncertainty associated with LUC emissions. Nevertheless, these observation-based constraints of
822 the carbon cycle and historical carbon budget are essentially the only means to evaluate carbon
823 cycle aspects of the ESMs at the global scale including the strength of the terrestrial CO₂
824 fertilization effect. In the near future, availability of model output from the sixth phase of CMIP
825 (CMIP6) will allow a comparison of the simulated aspects of the global carbon cycle and the
826 historical carbon budget from ESMs to observations-based estimates for the 1850-2014 period.
827 These data will allow a comparison of the rate of increase of the amplitude of globally-averaged
828 surface [CO₂] in models with observation-based estimates over a longer period. This should help
829 better constrain the strength of the terrestrial CO₂ fertilization effect, as it is represented in
830 models, in a somewhat more robust manner.

831

832 **6.0 Source code and data availability**

833 Source code for the complete CanESM4.2 model is an extremely complex set of FORTRAN
834 subroutines, with C preprocessor (CPP) directives, that reside in CCCma libraries. Unix shell
835 scripts process the model code for compilation based on CPP directives and several other
836 switches (e.g. those related to free-CO₂, specified-CO₂, and relaxed-CO₂ settings). As such, it is
837 extremely difficult to make the full model code available. However, selected model subroutines
838 related to specific physical and biogeochemical processes can be made available by either author
839 (vivek.arora@canada.ca, john.scinocca@canada.ca) upon agreeing to Environment and Climate
840 Change Canada's software licensing agreement available at
841 <http://collaboration.cmc.ec.gc.ca/science/rpn.comm/license.html>. Data used to produce plots and
842 figures can be obtained from the first author (vivek.arora@canada.ca).

843

844 **Copyright statement**

845 The works published in this journal are distributed under the Creative Commons Attribution 3.0
846 License. This license does not affect this Crown copyright work, which is re-usable under the
847 Open Government License (OGL). The Creative Commons Attribution 3.0 License and the OGL
848 are interoperable and do not conflict with, reduce or limit each other. ©Crown copyright 2015.

849

850 **Acknowledgements**

851 We would like to thank Joe Melton and Neil Swart for providing comments on an earlier version
852 of this paper. We also thank the three anonymous reviewers for their constructive and helpful
853 comments.

854

Formatted: Font: Not Bold

Formatted: Font: Not Bold

855 **References**

- 856 [Arora, V. K. and Boer, G. J. \(2005\) A parameterization of leaf phenology for the terrestrial ecosystem](#)
857 [component of climate models, *Glob. Change Biol.*, 11, 39–59, doi:10.1111/j.1365-](#)
858 [2486.2004.00890.x.](#)
- 859 [Arora, V. K. and Boer, G. J. \(2014\) Terrestrial ecosystems response to future changes in climate and](#)
860 [atmospheric CO₂ concentration, *Biogeosciences*, 11, 4157-4171, doi:10.5194/bg-11-](#)
861 [4157-2014](#)Arora, V. K. and Boer, G. J. (2014) Terrestrial ecosystems response to future
862 [changes in climate and atmospheric CO₂ concentration, *Biogeosciences Discuss.*, 11,](#)
863 [3581-3614, doi:10.5194/bgd-11-3581-2014.](#)
- 864 [Arora, V. K., G. J. Boer, J. R. Christian, C. L. Curry, K. L. Denman, K. Zahariev, G. M. Flato, J. F.](#)
865 [Scinocca, W. J. Merryfield, and W. G. Lee \(2009\) The effect of terrestrial photosynthesis](#)
866 [down-regulation on the 20th century carbon budget simulated with the CCCma Earth](#)
867 [System Model, *J. Clim.*, 22, 6066-6088.](#)
- 868 [Arora, V. K., G. J. Boer, P. Friedlingstein, M. Eby, C. D. Jones, J. R. Christian, G. Bonan, L. Bopp,](#)
869 [V. Brovkin, P. Cadule, T. Hajima, T. Ilyina, K. Lindsay, J. F. Tjiputra, T. Wu \(2013\)](#)
870 [Carbon-Concentration and Carbon-Climate Feedbacks in CMIP5 Earth System Models,](#)
871 [*Journal of Climate*, Vol. 26, Iss. 15, pp. 5289-5314.](#)
- 872 [Arora, V. K., J. F. Scinocca, G. J. Boer, J. R. Christian, K. L. Denman, G. M. Flato, V. V. Kharin, W.](#)
873 [G. Lee, and W. J. Merryfield \(2011\) Carbon emission limits required to satisfy future](#)
874 [representative concentration pathways of greenhouse gases, *Geophys. Res. Lett.*, 38,](#)
875 [L05805, doi:10.1029/2010GL046270.](#)
- 876 [Arora, V.K. and G.J. Boer \(2010\) Uncertainties in the 20th century carbon budget associated with](#)
877 [land use change, *Global Change Biology*, 16\(12\), 3327-3348.](#)
- 878 [Bartlett, P. A., Mackay, M. D., and Verseghy, D. L. \(2006\) Modified snow algorithms in the Canadian](#)
879 [Land Surface Scheme: model runs and sensitivity analysis at three boreal forest stands,](#)
880 [*Atmos. Ocean*, 44, 207–222.](#)
- 881 [Bartlett, P. and Verseghy, D. \(2015\) Modified treatment of intercepted snow improves the](#)
882 [simulated forest albedo in the Canadian Land Surface Scheme, *Hydrol. Process.*, 29, 3208–](#)
883 [3226, doi:10.1002/hyp.10431.](#)
- 884 [Brown, R., Bartlett, P., Mackay, M., and Verseghy, D. \(2006\) Estimation of snow cover in CLASS for](#)
885 [SnowMIP, *Atmos. Ocean*, 44, 223–238.](#)

886 [Christian, J. R., and coauthors \(2010\) The global carbon cycle in the Canadian Earth system model](#)
887 [\(CanESM1\): Preindustrial control simulation, J. Geophys. Res., 115, G03014,](#)
888 [doi:10.1029/2008JG000920.](#)

889 [Ciais, P., C. Sabine, G. Bala, L. Bopp, V. Brovkin, J. Canadell, A. Chhabra, R. DeFries, J. Galloway,](#)
890 [M. Heimann, C. Jones, C. Le Quéré, R.B. Myneni, S. Piao and P. Thornton \(2013\) Carbon](#)
891 [and Other Biogeochemical Cycles. In: Climate Change 2013: The Physical Science Basis.](#)
892 [Contribution of Working Group I to the Fifth Assessment Report of the Intergovernmental](#)
893 [Panel on Climate Change \[Stocker, T.F., D. Qin, G.-K. Plattner, M. Tignor, S.K. Allen, J.](#)
894 [Boschung, A. Nauels, Y. Xia, V. Bex and P.M. Midgley \(eds.\)\]. Cambridge University](#)
895 [Press, Cambridge, United Kingdom and New York, NY, USA.](#)

896 [da Rocha, H.R., M.L. Goulden, S.D. Miller, M.C. Menton, L.D.V.O. Pinto, H.C. De Freitas, and](#)
897 [A.M.E. Silva Figueira \(2004\): Seasonality of water and heat fluxes over a tropical forest](#)
898 [in eastern Amazonia, Ecological Applications, 14\(4\) Supplement, S22-S32.](#)

899 [Friedlingstein, P., P. Cox, R. Betts, L. Bopp, W. von Bloh, V. Brovkin, P. Cadule, S. Doney, M. Eby,](#)
900 [I. Fung, G. Bala, J. John, C. Jones, F. Joos, T. Kato, M. Kawamiya, W. Knorr, K. Lindsay,](#)
901 [H. D. Matthews, T. Raddatz, P. Rayner, C. Reick, E. Roeckner, K.-G. Schnitzler, R.](#)
902 [Schnur, K. Strassmann, A. J. Weaver, C. Yoshikawa, N. Zeng. 2006: Climate-carbon](#)
903 [cycle feedback analysis: Results from the C4MIP model intercomparison, J. Clim., 19\(14\),](#)
904 [3337-3353.](#)

905 [G. C. Hurtt, L. P. Chini, S. Frolking, R. A. Betts, J. Feddema, G. Fischer, J. P. Fisk, K. Hibbard, R. A.](#)
906 [Houghton, A. Janetos, C. D. Jones, G. Kindermann, T. Kinoshita, Kees Klein Goldewijk,](#)
907 [K. Riahi, E. Shevliakova, S. Smith, E. Stehfest, A. Thomson, P. Thornton, D. P. van](#)
908 [Vuuren, Y. P. Wang \(2011\) Harmonization of land-use scenarios for the period 1500-](#)
909 [2100: 600 years of global gridded annual land-use transitions, wood harvest, and resulting](#)
910 [secondary lands. Climatic Change, 109, 117-161, doi:10.1007/s10584-011-0153-2.](#)

911 [Garnaud, C., L. Sushama, V. K. Arora \(2014\) The effect of driving climate data on the simulated](#)
912 [terrestrial carbon pools and fluxes over North America, International Journal of](#)
913 [Climatology 34 \(4\), 1098-1110.](#)

914 [Gillett, N. P., V. K. Arora, D. Matthews, M. R. Allen \(2013\) Constraining the Ratio of Global](#)
915 [Warming to Cumulative CO2 Emissions Using CMIP5 Simulations. Journal of Climate,](#)
916 [Vol. 26, Iss. 18, pp. 6844-6858.](#)

917 [Gourdji, S. M., K. L. Mueller, V. Yadav, D. N. Huntzinger, A. E. Andrews, M. Trudeau, G. Petron, T.](#)
918 [Nehrkorn, J. Eluszkiewicz, J. Henderson, D. Wen, J. Lin, M. Fischer, C. Sweeney, and A.](#)
919 [M. Michalak \(2012\) North American CO2 exchange: inter-comparison of modeled](#)
920 [estimates with results from a fine-scale atmospheric inversion, Biogeosciences, 9, 457–](#)
921 [475, doi:10.5194/bg-9-457-2012.](#)

922 [Hoffman, F. M., J. T. Randerson, V. K. Arora, Q. Bao, P. Cadule, D. Ji, C. D. Jones, M. Kawamiya,](#)
923 [S. Khatiwala, K. Lindsay, A. Obata, E. Shevliakova, K. D. Six, J. F. Tjiputra, E. M.](#)
924 [Volodin, and T. Wu \(2014\) Causes and implications of persistent atmospheric](#)
925 [carbondioxide biases in Earth System Models, J. Geophys. Res. Biogeosci., 119, 141–162,](#)
926 [doi:10.1002/2013JG002381.](#)

927 [Houghton, R.A. 2008. Carbon Flux to the Atmosphere from Land-Use Changes: 1850-2005. In](#)
928 [TRENDS: A Compendium of Data on Global Change. Carbon Dioxide Information](#)
929 [Analysis Center, Oak Ridge National Laboratory, U.S. Department of Energy, Oak Ridge,](#)
930 [Tenn., U.S.A.](#)

931 [Jones, C., E. Robertson, V. Arora, P. Friedlingstein, E. Shevliakova, L. Bopp, V. Brovkin, T. Hajima,](#)
932 [E. Kato, M. Kawamiya, S. Liddicoat, K. Lindsay, C.H. Reick, C. Roelandt, J.](#)
933 [Segschneider, J. Tjiputra \(2013\) Twenty-First-Century Compatible CO2 Emissions and](#)
934 [Airborne Fraction Simulated by CMIP5 Earth System Models under Four Representative](#)
935 [Concentration Pathways. Journal of Climate, Vol. 26, Iss. 13, pp. 4398-4413.](#)

936 [Keeling, C. D., Chin, J. F. S. & Whorf, T. P. \(1996\) Increased activity of northern vegetation inferred](#)
937 [from atmospheric CO2 measurements. Nature 382, 146–149.](#)

938 [Khatiwala, S., F. Primeau, and T. Hall \(2009\) Reconstruction of the history of anthropogenic CO2](#)
939 [concentrations in the ocean. Nature, 462, 346–349.](#)

940 [Knol, M. J., W. R. Pestman, and D. E. Grobbee \(2011\) The \(mis\)use of overlap of confidence](#)
941 [intervals to assess effect modification, Eur. J. Epidemiol., 26\(4\), 253–254.](#)

942 [Knorr, W. \(2009\) Is the airborne fraction of anthropogenic CO2 emissions increasing?, Geophys. Res.](#)
943 [Lett., 36, L21710, doi:10.1029/2009GL040613.](#)

944 [Le Quéré, C., Moriarty, R., Andrew, R. M., Peters, G. P., Ciais, P., Friedlingstein, P., Jones, S. D.,](#)
945 [Sitch, S., Tans, P., Arneeth, A., Boden, T. A., Bopp, L., Bozec, Y., Canadell, J. G., Chini,](#)
946 [L. P., Chevallier, F., Cosca, C. E., Harris, I., Hoppema, M., Houghton, R. A., House, J. I.,](#)
947 [Jain, A. K., Johannessen, T., Kato, E., Keeling, R. F., Kitidis, V., Klein Goldewijk, K.,](#)
948 [Koven, C., Landa, C. S., Landschützer, P., Lenton, A., Lima, I. D., Marland, G., Mathis, J.](#)

949 [T., Metzl, N., Nojiri, Y., Olsen, A., Ono, T., Peng, S., Peters, W., Pfeil, B., Poulter, B.,](#)
950 [Raupach, M. R., Regnier, P., Rödenbeck, C., Saito, S., Salisbury, J. E., Schuster, U.,](#)
951 [Schwinger, J., Séférian, R., Segschneider, J., Steinhoff, T., Stocker, B. D., Sutton, A. J.,](#)
952 [Takahashi, T., Tilbrook, B., van der Werf, G. R., Viovy, N., Wang, Y.-P., Wanninkhof,](#)
953 [R., Wiltshire, A., and Zeng, N. \(2015\) Global carbon budget 2014, Earth Syst. Sci. Data,](#)
954 [7, 47-85, doi:10.5194/essd-7-47-2015.](#)

955 [Ma, X., von Salzen, K., and Li, J. \(2008\) Modelling sea salt aerosol and its direct and indirect effects](#)
956 [on climate, Atmos. Chem. Phys., 8, 1311–1327, doi:10.5194/acp-8-1311-2008.](#)

957 [McGuire, A. D., J. M. Melilli, and L. A. Joyce \(1995\): The role of nitrogen in the response of forest](#)
958 [net primary productivity to elevated atmospheric carbon dioxide, Annual Reviews of](#)
959 [Ecology and Systematics, 26, 473-503.](#)

960 [Medlyn, B. E., F. -W. Badeck, D. G. G. De Pury, C. V. M. Barton, M. Broadmeadow, R. Ceulemans,](#)
961 [P. De Angelis, M. Forstreuter, M. E. Jach, S. Kellomäki, E. Laitat, M. Marek, S. Philippot,](#)
962 [A. Rey, J. Strassmeyer, K. Laitinen, R. Liozon, B. Portier, P. Roberntz, K. Wang, P. G.](#)
963 [Jstbid \(1999\): Effects of elevated \[CO₂\] on photosynthesis in European forest species: a](#)
964 [meta-analysis of model parameters. Plant, Cell & Environment, 22, 1475–1495.](#)

965 [Melton, J. R. and Arora, V. K. \(2014\) Sub-grid scale representation of vegetation in global land](#)
966 [surface schemes: implications for estimation of the terrestrial carbon sink, Biogeosciences,](#)
967 [11, 1021-1036, doi:10.5194/bg-11-1021-2014.](#)

968 [Melton, J. R. and Arora, V. K. \(2014\) Sub-grid scale representation of vegetation in global land](#)
969 [surface schemes: implications for estimation of the terrestrial carbon sink, Biogeosciences,](#)
970 [11, 1021-1036, doi:10.5194/bg-11-1021-2014.](#)

971 [Melton, J. R., Shrestha, R. K., and Arora, V. K. \(2015\) The influence of soils on heterotrophic](#)
972 [respiration exerts a strong control on net ecosystem productivity in seasonally dry](#)
973 [Amazonian forests, Biogeosciences, 12, 1151-1168, doi:10.5194/bg-12-1151-2015.](#)

974 [Namazi, M., von Salzen, K., and Cole, J. N. S. \(2015\) Simulation of black carbon in snow and its](#)
975 [climate impact in the Canadian Global Climate Model, Atmos. Chem. Phys. Discuss., 15,](#)
976 [18839-18882, doi:10.5194/acpd-15-18839-2015.](#)

977 [Peng, Y., Arora, V. K., Kurz, W. A., Hember, R. A., Hawkins, B. J., Fyfe, J. C., and Werner, A. T.](#)
978 [\(2014\) Climate and atmospheric drivers of historical terrestrial carbon uptake in the](#)
979 [province of British Columbia, Canada, Biogeosciences, 11, 635-649, doi:10.5194/bg-11-](#)
980 [635-2014.](#)

981 [Peng, Y., von Salzen, K., and Li, J. \(2012\) Simulation of mineral dust aerosol with Piecewise Log-](#)
982 [normal Approximation \(PLA\) in CanAM4-PAM, Atmos. Chem. Phys., 12, 6891–6914, 30](#)
983 [doi:10.5194/acp-12-6891-2012.](#)

984 [Phillips, O. L. and S. L. Lewis \(2014\) Evaluating the tropical forest carbon sink, Global Change](#)
985 [Biology \(2014\) 20, 2039–2041, doi: 10.1111/gcb.12423.](#)

986 [Pongratz, J., Reick, C. H., Houghton, R. A., and House, J. I. \(2014\) Terminology as a key uncertainty](#)
987 [in net land use and land cover change carbon flux estimates, Earth Syst. Dynam., 5, 177-](#)
988 [195, doi:10.5194/esd-5-177-2014.](#)

989 [Ramankutty, N., H. K. Gibbs, F. Archard, R. DeFries, J. A. Foley, and R. A. Houghton \(2007\):](#)
990 [Challenges to estimating carbon emissions from tropical deforestation , Global Change](#)
991 [Biology, 13\(1\), 51-66.](#)

992 [Randerson, J. T., Thompson, M. V., Conway, T. J., Fung, I. Y. & Field, C. B. \(1997\) The contribution](#)
993 [of terrestrial sources and sinks to trends in the seasonal cycle of atmospheric carbon](#)
994 [dioxide. Glob. Biogeochem. Cycles 11, 535–560.](#)

995 [Schimel, D., Stephens, B. B., and Fisher, J. B.: Effect of increasing CO2 on the terrestrial carbon](#)
996 [cycle \(2015\) Proceedings of the National Academy of Science U.S.A., 112, 436–441,](#)
997 [doi:10.1073/pnas.1407302112, 2015.](#)

998 [Sturm, M., Holmgren, J., König, M., and Morris, K. \(1997\) The thermal conductivity of seasonal](#)
999 [snow, J. Glaciol., 43, 26–41.](#)

1000 [Tabler, R. D., Benson, C. S., Santana, B. W., and Ganguly, P. \(1990\) Estimating snow transport from](#)
1001 [30 wind speed records: estimates versus measurements at Prudhoe Bay, Alaska, in: Proc.](#)
1002 [58th Western Snow Conf., Sacramento, CA, 61–78.](#)

1003 [Taylor, Karl E., Ronald J. Stouffer, Gerald A. Meehl, 2012: An Overview of CMIP5 and the](#)
1004 [Experiment Design. Bull. Amer. Meteor. Soc., 93, 485–498.](#)

1005 [Verseghy, D. L. \(2012\) CLASS-the Canadian land surface scheme \(version 3.6\)—technical](#)
1006 [documentation. Internal report, Climate Research Division, Science and Technology](#)
1007 [Branch, Environment Canada \(Downsview, Toronto, Ontario\)](#)

1008 [von Salzen, K. \(2006\) Piecewise log-normal approximation of size distributions for aerosol](#)
1009 [modelling, Atmos. Chem. Phys., 6, 1351–1372, doi:10.5194/acp-6-1351-2006.](#)

1010 [von Salzen, K., and Coauthors, 2013: The Canadian fourth generation atmospheric global climate](#)
1011 [model \(CanAM4\). Part I: Representation of physical processes. Atmos. Ocean, 51,](#)
1012 [doi:10.1080/07055900.2012.75561.](#)

1013 [Wei, X., M. Shao, W. Gale and L. Li \(2014\) Global pattern of soil carbon losses due to the conversion](#)
1014 [of forests to agricultural land, Scientific Reports 4, Article number: 4062 \(2014\)](#)
1015 [doi:10.1038/srep04062.](#)

1016 [Zaehle, S., Medlyn, B. E., De Kauwe, M. G., Walker, A. P., Dietze, M. C., Hickler, T., Luo, Y.,](#)
1017 [Wang, Y.-P., El-Masri, B., Thornton, P., Jain, A., Wang, S., Warlind, D., Weng, E.,](#)
1018 [Parton, W., Iversen, C. M., Gallet-Budynek, A., McCarthy, H., Finzi, A., Hanson, P. J.,](#)
1019 [Prentice, I. C., Oren, R., and Norby, R. \(2014\) Evaluation of 11 terrestrial carbon–nitrogen](#)
1020 [cycle models against observations from two temperate Free-Air CO2 Enrichment studies,](#)
1021 [New Phytologist, 202, 803–822, doi:10.1111/nph.12697.](#)

1022 [Zeng, N., Zhao, F., Collatz, G. J., Kalnay, E., Salawitch, R. J., West, T. O., Guanter, L. \(2014\) .](#)
1023 [Agricultural Green Revolution as a driver of increasing atmospheric CO2 seasonal](#)
1024 [amplitude, Nature, 515\(7527\), 394-397.](#)

1025 [Zobler, L. 1986. A World Soil File for Global Climate Modelling. NASA Technical Memorandum](#)
1026 [87802. NASA Goddard Institute for Space Studies, New York, New York, U.S.A.](#)

1027

1028

1029 Table 1: Summary of simulations performed for this study and the forcings used.

Simulation	1petCO2	esmhistorical	esmhistorical_noluc
Simulation details	1% per year increasing CO ₂ simulation	1850-2005 historical simulation based on CMIP5 protocol	1850-2005 historical simulation based on CMIP5 protocol, but with no anthropogenic land use change
<u>Purpose</u>	<u>To allow comparison of CanESM4.2 with CMIP5 models especially in terms of its land carbon uptake</u>	<u>To compare simulated aspects of the global carbon cycle and historical carbon budget with observation-based estimates</u>	<u>To diagnose LUC emissions by differencing atmosphere-land CO₂ flux between historical simulations with and without LUC.</u>
Length	140 years	156 years	
CO ₂ forcing	285 ppm at the start of the simulation and 1140 ppm after 140 years.	Historical CO ₂ forcing	
Land cover forcing	Land cover corresponds to its 1850 state	Land cover evolution is based on increase in crop area over the historical period	Land cover corresponds to its 1850 state
Non-CO ₂ greenhouse gases forcing	Concentration of non-CO ₂ GHGs is specified at their 1850 levels.	Concentration of non-CO ₂ GHGs is specified and evolves over the historical period based on the CMIP5 protocol	
Aerosols forcing	Emissions of aerosols and their precursors are specified at their 1850 levels.	Emissions of aerosols and their precursors are specified and evolve over the historical period based on the CMIP5 protocol	

Formatted: Subscript

1030

1031

1032

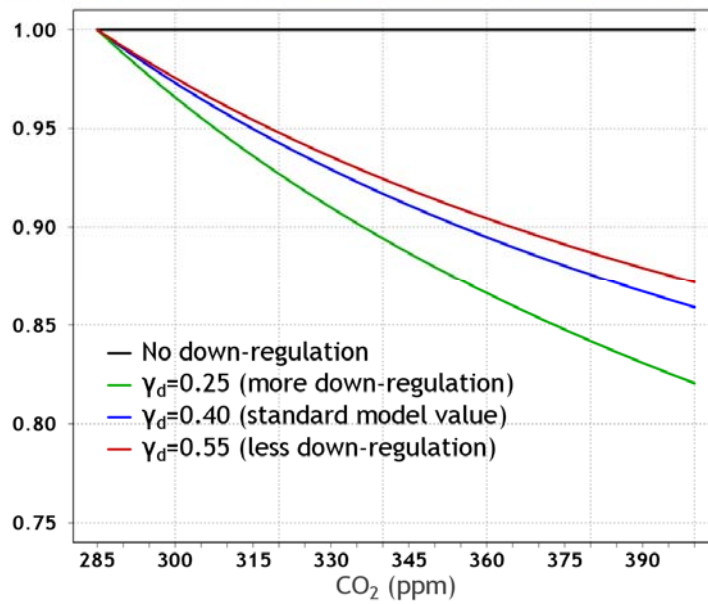
1033

1034

1035

1036

Down-regulation factor as a function of CO₂ concentration



1037

1038 | Figure 1: The behaviour of terrestrial photosynthesis down-regulation scalar $\xi(C)$ (equation 124)

1039 for $\gamma_p=0.95$ and values of γ_d equal to 0.25, 0.4 and 0.55 that are used in CanESM4.2 simulations.

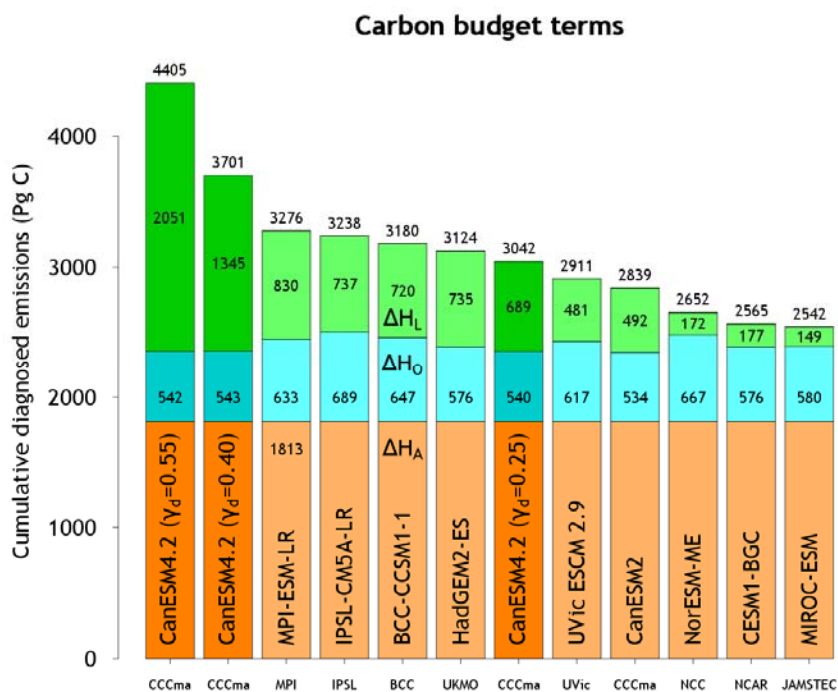
1040

1041

1042

1043

1044



1045

1046

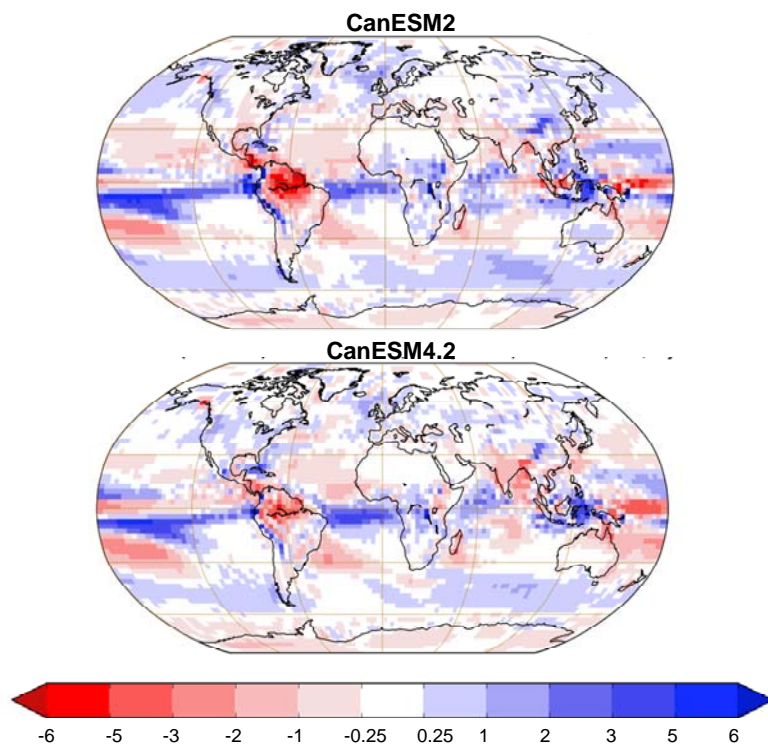
1047 Figure 2: Components of the carbon budget equation (8) that make up cumulative diagnosed
 1048 emissions based on results from the fully-coupled 1pctCO2 experiment. Results shown are from
 1049 eight CMIP5 models that participated in the Arora et al. (2013) study and from three CanESM4.2
 1050 simulations (shown in darker colours) for three different strengths of the terrestrial CO₂
 1051 fertilization effect.

1052

1053

1054

Model minus Xie and Arkin precipitation
averaged over the 1979-1998 period (mm/day)



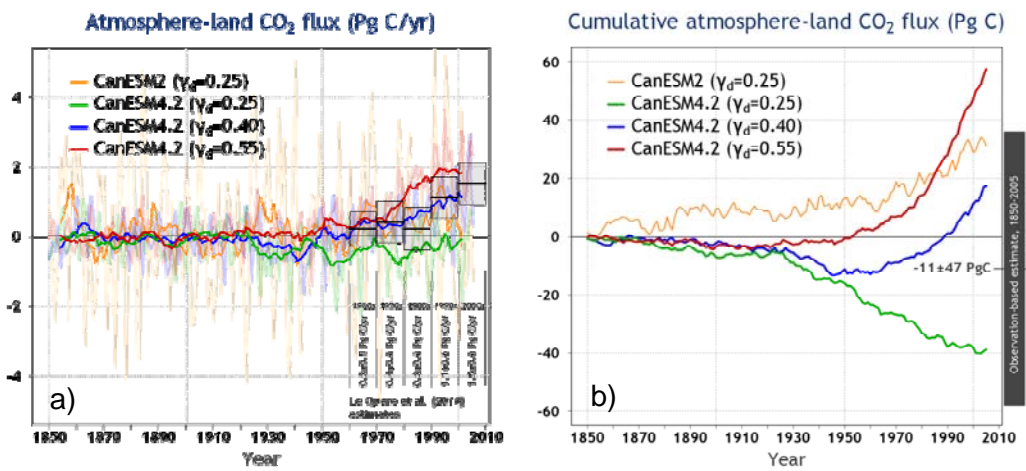
1055

1056

1057 Figure 3: CanESM2 (panel a) and CanESM4.2 (panel b, $\gamma_d=0.40$) precipitation anomalies
1058 compared to the observation-based estimates from CPC Merged Analysis of Precipitation
1059 (CMAP) based on Xie and Arkin (1997) averaged over the 1979–1998 period.

1060

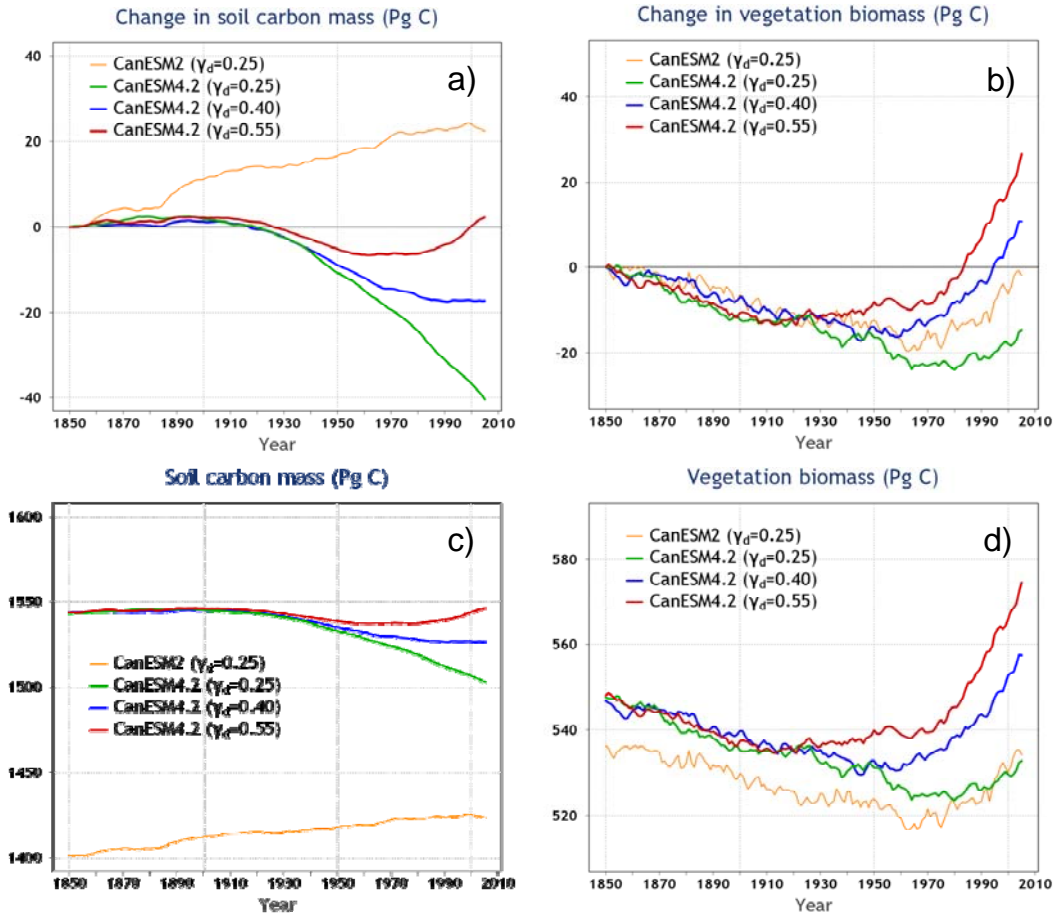
1061
1062
1063
1064
1065



1066

1067 Figure 4: Atmosphere-land CO₂ flux (F_L) (panel a) and its cumulative values \tilde{F}_L (panel b) from
1068 CanESM2 and the three CanESM4.2 historical 1850-2005 simulations for different strengths of
1069 the terrestrial CO₂ fertilization effect. In panel (a) the observation-based estimates of F_L and their
1070 uncertainty, show via boxes, for the decades of 1960, 1970, 1980, 1990 and 2000 are reproduced
1071 from Le Quéré et al. (2015). The bold lines in panel (a) are the 10-year moving averages of the
1072 annual F_L values which are shown in light colours. The results from CanESM2 and CanESM4.2
1073 are the average of the two ensemble members.

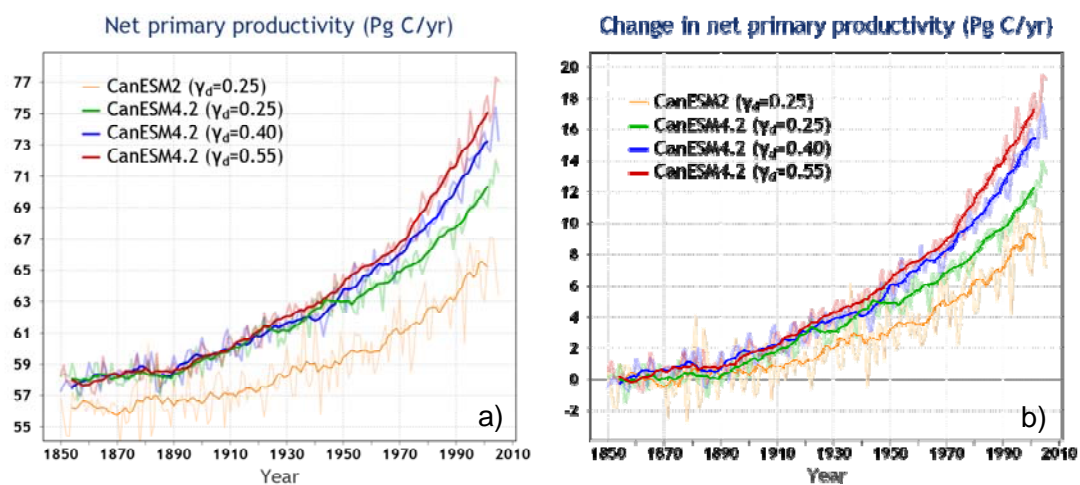
1074
1075



1078 Figure 5: Change in and absolute values of global soil carbon and vegetation biomass amounts
 1079 from CanESM2 and the three CanESM4.2 historical 1850-2005 simulations with different
 1080 strengths of the terrestrial CO_2 fertilization effect. The results shown in all panels are the average
 1081 of the two ensemble members.

1085

1086



1087

1088 Figure 6: Absolute values of (panel a), and change in (panel b), net primary productivity (NPP)
1089 from CanESM2 and the three CanESM4.2 historical 1850-2005 simulations with different
1090 strengths of the terrestrial CO₂ fertilization effect. The thin lines show the ensemble-mean based
1091 on results from the two ensemble members and the bold lines are their 10-year moving averages.

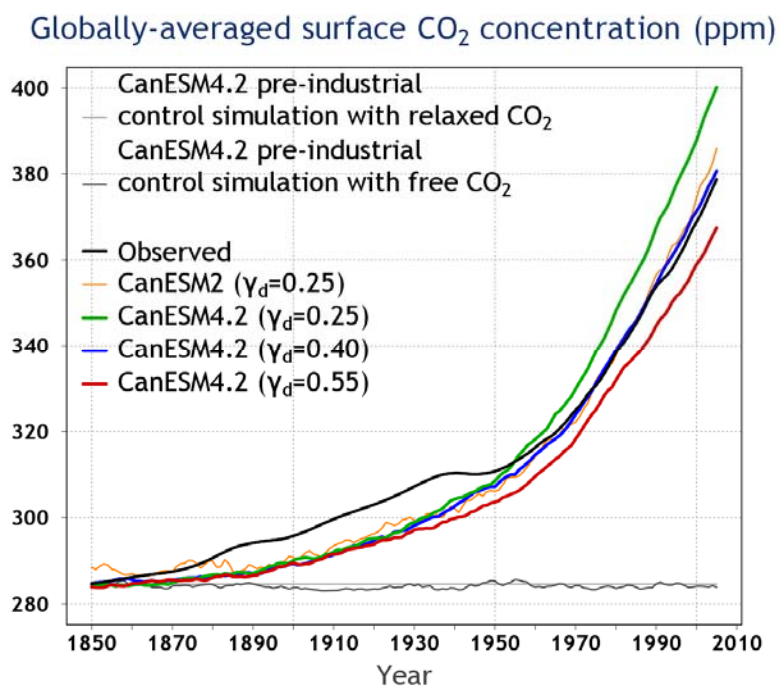
1092

1093

1094

1095

1096

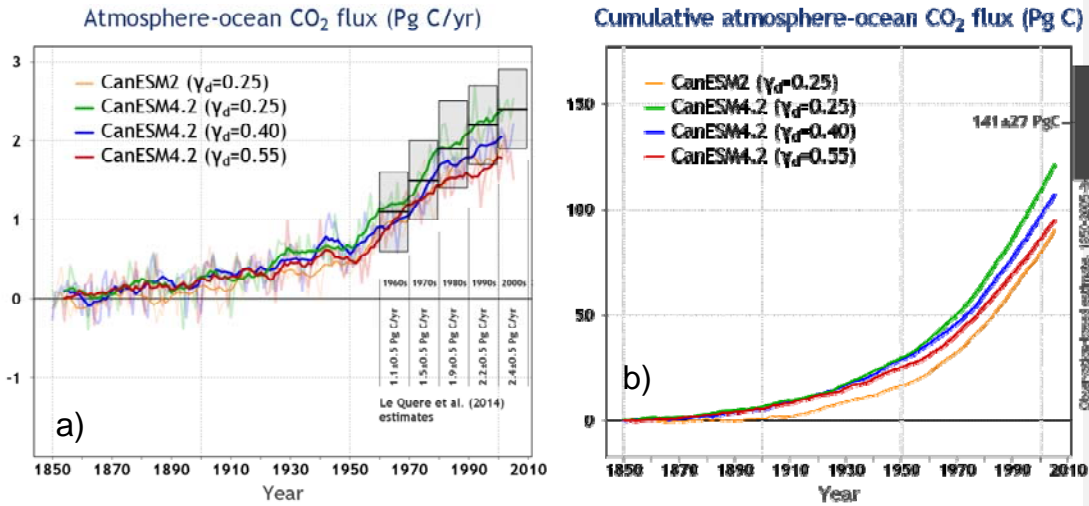


1097

1098 Figure 7: Simulated globally-averaged surface atmospheric CO₂ concentration from CanESM2
1099 and the three CanESM4.2 historical 1850-2005 simulations with different strengths of the
1100 terrestrial CO₂ fertilization effect. The observation-based concentration is shown in black. Also
1101 shown is the CO₂ concentration of 284.6 ppm used in CanESM4.2's pre-industrial simulation
1102 with "specified" CO₂ in the relaxed-CO₂ configuration and the simulated concentration from the
1103 pre-industrial CanESM4.2 simulation with interactively determined CO₂.

1104

1105
1106
1107

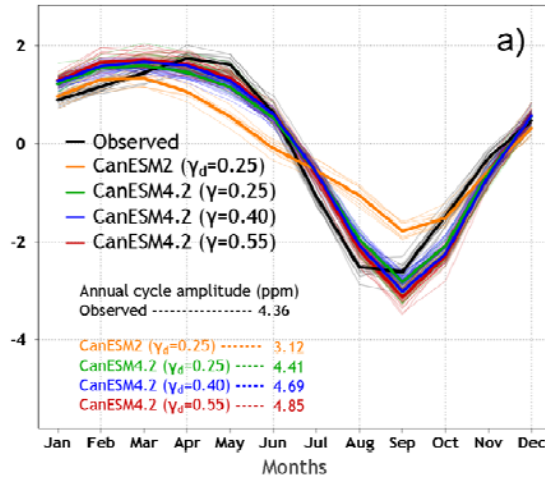


1108

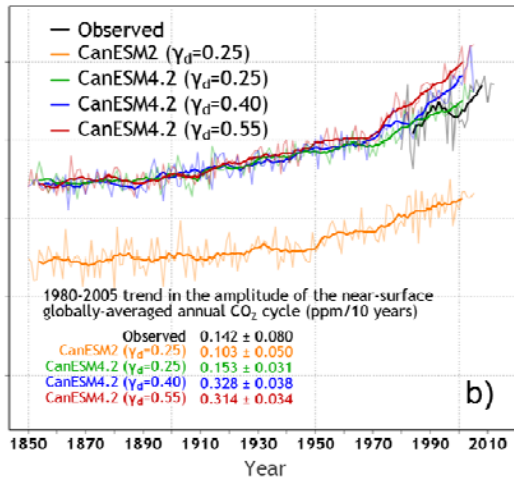
1109 Figure 8: Atmosphere-ocean CO₂ flux (F_O) (panel a) and its cumulative values \tilde{F}_O (panel b) from
1110 CanESM2 and the three CanESM4.2 historical 1850-2005 simulations for three different
1111 strengths of the terrestrial CO₂ fertilization effect. In panel (a) the observation-based estimates of
1112 F_O and their uncertainty, show via boxes, for the decades of 1960, 1970, 1980, 1990 and 2000 are
1113 reproduced from Le Quéré et al. (2015). The bold lines in panel (a) are the 10-year moving
1114 averages of the annual F_L values which are shown in light colours. The results from CanESM2
1115 and CanESM4.2 are the average of the two ensemble members.

1116
1117

Monthly CO₂ cycle trend-adjusted anomalies (ppm) 1991-2000



Amplitude of the globally-averaged annual CO₂ cycle (ppm)

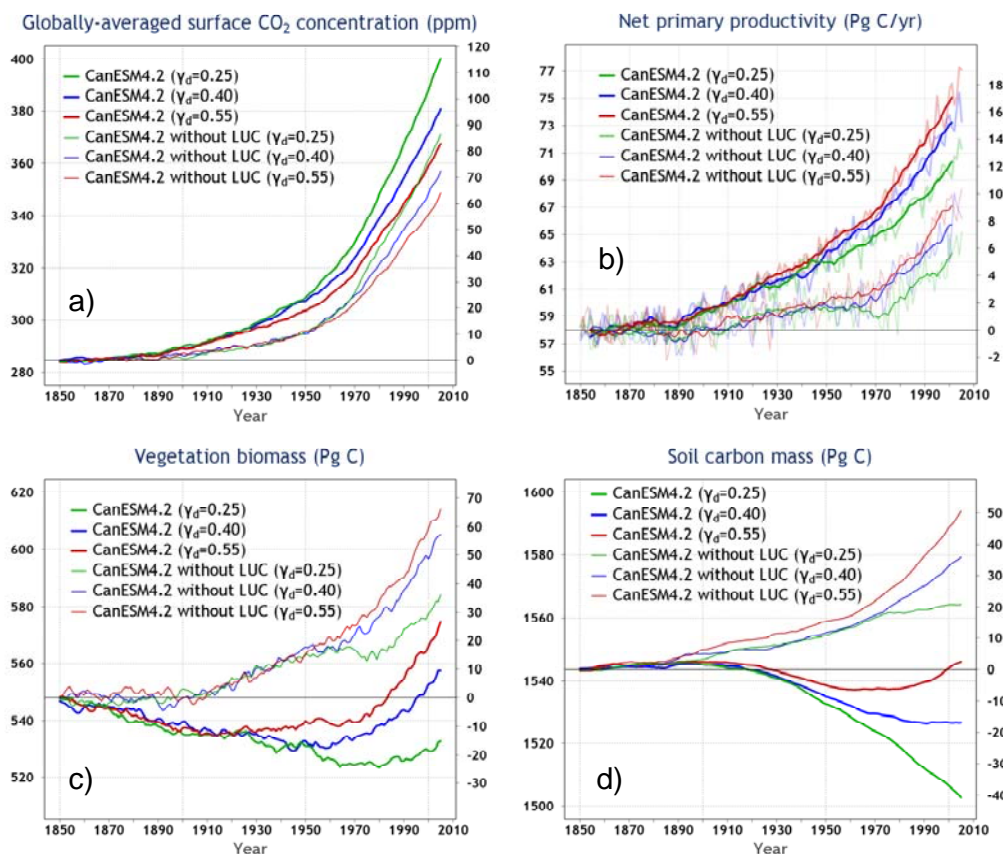


1118

1119 Figure 9: The annual cycle of trend-adjusted globally-averaged near-surface monthly [CO₂]
 1120 anomalies from CanESM2, the versions of CanESM4.2 for three different strengths of the CO₂
 1121 fertilization effect and observation-based estimates for the 1991-2000 period (panel a). Panel (b)
 1122 shows the time series of the amplitude of the annual cycle of the trend adjusted globally-averaged
 1123 near-surface monthly [CO₂] anomalies for corresponding model and observation-based estimates.
 1124 The bold lines are 10-year moving averages and the thin lines for model results are the average of
 1125 results from two ensemble members.

1126

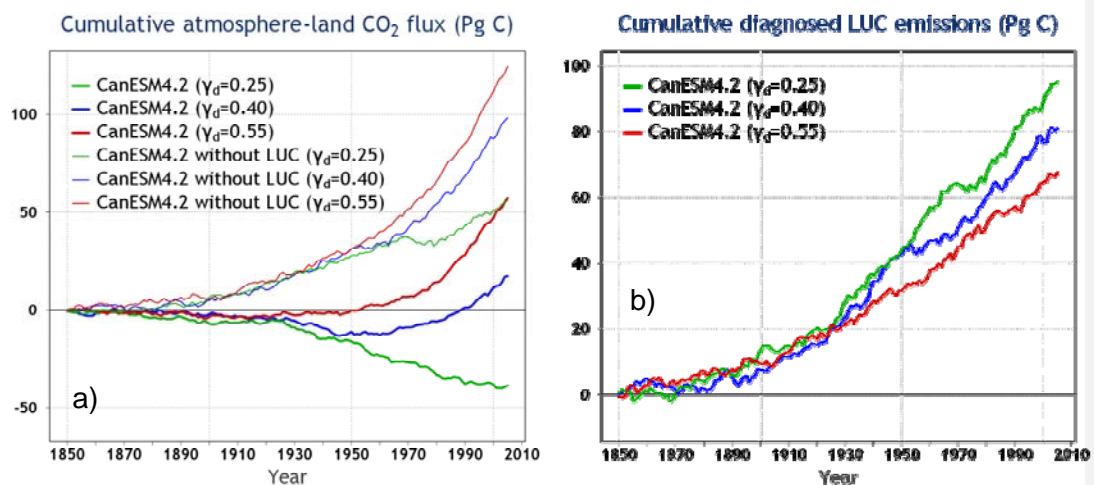
1127
1128



1129
1130 Figure 10: Comparison of CanESM4.2 simulations with and without implementation of
1131 anthropogenic land use change over the historical period for three different strengths of the
1132 terrestrial CO₂ fertilization effect: a) Globally-averaged annual surface atmospheric CO₂
1133 concentration, b) net primary productivity, c) global vegetation biomass, and c) global soil carbon
1134 mass. All lines are the average of results from two ensemble members. Additionally, in panel (b)
1135 the bold lines are the 10-year moving averages.

1136
1137

1138
1139



1140
1141
1142
1143
1144
1145
1146
1147
1148
1149
1150

Figure 11: Comparison of simulated cumulative atmosphere-land CO₂ flux from CanESM4.2 simulations with and without implementation of anthropogenic land use change over the historical period for three different strengths of the terrestrial CO₂ fertilization (panel a). Panel (b) shows the cumulative diagnosed LUC emissions calculated using equation (10) as the difference between cumulative atmosphere-land CO₂ flux from simulations with and without LUC shown in panel (a). All lines are the average of results from two ensemble members.